NASA-TP-2338 19840018715

NASA Technical Paper 2338

July 1984

Effects of Alloy Composition on Cyclic Flame Hot-Corrosion Attack of Cast Nickel-Base Superalloys at 900° C

Daniel L. Deadmore

NASA

NASA
Technical
Paper
2338

1984

Effects of Alloy Composition on Cyclic Flame Hot-Corrosion Attack of Cast Nickel-Base Superalloys at 900° C

Daniel L. Deadmore

Lewis Research Center
Cleveland, Ohio

National Aeronautics
and Space Administration

**Scientific and Technical
Information Branch**

Summary

The effects of Cr, Al, Ti, Mo, Ta, Nb, and W content on the hot corrosion of nickel-base alloys were investigated. The alloys were chosen to cover nearly the range of commercial alloy compositions. They were tested in a Mach 0.3 flame with 0.5 ppmw sodium at a temperature of 900° C. The degree of attack was estimated by four methods: change in metal diameter, loss of cross-sectional area, descaled weight loss, and change in the inductance of a solenoid coil with a test sample as a core. The first three measurements are destructive and were made only at the end of testing (300 1-hr cycles). The coil measurement is a nondestructive method. By using coil measurements, the corrosion resistance of these alloys could be predicted from short-time testing.

The best corrosion resistance was achieved when the Cr content was greater than 12 wt %. However, some lower-Cr-content alloys (<10 wt %) exhibited reasonable resistance provided that the Al content was less than 2.5 wt % and the Ti content was less than 4 wt %. The effects of W, Ta, Mo, and Nb content on the hot-corrosion resistance varied depending on the Al and Ti content. Several commercial alloy compositions were also tested and the corrosion attack was measured. Predicted attack was calculated for these alloys from derived regression equations and was in reasonable agreement with that experimentally measured. The regression equations were derived from measurements made on alloys in a one-quarter replicate of a 2^7 statistical design alloy composition experiment. These regression equations represent a simple linear model and are only a very preliminary analysis of the data needed to provide insights into the experimental method.

Introduction

Nickel-based, cast superalloys used in combustion turbine engines can experience high-temperature corrosive attack. Many factors influence the degree of such attack. A few of the more widely recognized factors are amount and type of impurities in the air and fuel (such as alkali, metal ions, and sulfur), alloy composition, combustion chamber pressure, deposition rates of impurity products, and temperature. Most of these factors are closely interrelated, and their roles in the hot-corrosion process have been the subject of numerous recent investigations (refs. 1 to 5). Alloy compositional effects are probably the least understood because of the synergisms involved. As noted by Stringer (ref. 6), about the only generally agreed upon conclusion regarding the effects of alloying elements in hot corrosion is that high chromium content (at least 14 wt %) is required for consistent hot-corrosion resistance. However, beyond this conclusion there is no general agreement on the effects of other elements, such as Ti, Nb, Al, Mo, Ta, and W (refs. 7 to 12).

In the work reported herein, the susceptibility of 96 cast nickel-base superalloy samples to sodium-sulfate-induced hot-corrosion attack was investigated. A one-quarter replicate of a 2^7 factorial design experiment was run to study seven compositional variables (viz, Cr, Al, Ti, Mo, Nb, W, and Ta) at two concentration levels each. In addition to the 32 samples in the one-quarter replicate, 18 other compositions from the factorial design were also included together with six compositional variations outside the design and eight duplicates. An additional group of 16 samples was tested to provide complementary compositional data. Finally 16 commercial alloys were tested to assess the compositional-effect conclusions that were reached on the basis of preliminary statistical analysis of the factorial design experimental results. The alloys were tested for 300 1-hour cycles at 900° C in a Mach 0.3 burner rig flame containing 0.5 ppmw sodium. Corrosion attack was assessed by several methods. At 15-cycle intervals the inductance of a coil with the test specimen as the core was measured (ref. 13). After 300 cycles the cross-sectional area and diameter of the unaffected metal at the center of the hot zone were measured. Also, the specimens were electrolytically descaled and the weight change was determined. The descaled specimens were visually examined and the mode of attack recorded.

A complete statistical analysis of the experimental results will be the subject of a future publication. The preliminary analysis of the results presented herein indicated that the best resistance was achieved when the chromium content was greater than 12 wt %. However, some lower-Cr-content alloys (<10 wt %) exhibited reasonable resistance provided that the Al content was less than 2.5 wt % and the Ti content was less than 4 wt %. Also, the effect of W, Ta, Mo, and Nb content on hot-corrosion varied depending on the Al and Ti content.

Furnace cyclic oxidation testing and a statistical analysis of the one-quarter replicate of the 2^7 design alloys have already been reported (ref. 14). The effect of substituting Co for Ni on the hot-corrosion attack resistance of U700 and MAR-M 247 alloys is also reported.

Test Procedures

Alloy Compositions and Test Specimens

Test samples for the factorial design were cast nickel-base γ-γ' alloys with fixed levels of Co, C, Zr, and B. Alloy compositions containing high and low levels of Cr, Al, Ti, W, Nb, Ta, and Mo were prepared. The target levels and the actual levels determined by chemical analysis are given in table 1. The high and low levels of the seven alloy additions nearly spanned the concentrations found in commercial alloys. The general compositional locations of the 64 factorial design alloys (32 from the one-quarter replicate of 2^7, 18 additional, 8 duplicates, and 6 outside of the factorial design) based on the actual compositions are indicated in table 2. The actual compositions of all of the test bars are given in appendix A.

An additional group of 16 commerical alloy compositions was tested in this study. Their general compositional locations are given in table 3. The element level ranges used to place these alloys in positions in table 3 are also given and in some cases are different from those given in table 1. This was necessary because some of the commercial alloy compositions fall outside the element levels used for the factorial design alloys. The two TAZ-8A bars represent two actual compositions supplied by different vendors. Five Udimet 700 (U700) bars were tested: bars 5, 88, and 91 were duplicates and bars 4 and 10 were also duplicates but of a slightly different composition. The actual compositions of these bars are given in appendix A. Several specimens were tested in which Co was substituted at several levels for part of the Ni in commerical U700 and MAR-M 247 alloys. The actual compositions are given in appendix A.

Test specimens were prepared by vacuum induction melting and frame casting. The as-cast corrosion test bars (fig. 1) were wedge shaped and nominally 12.7 mm in diameter. These bars were machined to 12.4-mm-diameter test specimens, but the flat wedge faces were in the as-cast condition.

Corrosion Measurement Methods

To assess the degree of corrosive attack, four separate measurements were made: metal diameter, metal cross-sectional area, descaled weight, and inductance coil measurements. The first three measurements require destruction of the sample and thus were made only at the end of the testing. The last measurement is nondestructive and was made at various intervals during the course of the testing. The samples were photographed after 200 cycles of testing, and a visual examination of each descaled specimen was recorded after 300 cycles.

TABLE 1.—CONCENTRATION LEVELS OF ELEMENTS IN FACTORIAL DESIGN EXPERIMENT ALLOYS

(a) Element varied

Element	Low level		High level	
	Target	Actual	Target	Actual
	Content, wt %			
Al	2.1 – 2.3	1.7 – 3.3	5.6 – 6.3	5.0 – 7.2
Cr	7.9 – 9.3	6.1 – 9.4	14.5 – 16.7	12.6 – 15.6
Ti	1.5 – 1.7	1.2 – 2	4.5 – 5.1	3.1 – 4.9
Mo	1.5 – 1.7	1.2 – 1.8	4.5 – 5.1	3.4 – 5
W	3.0 – 3.3	2.3 – 4.6	8.4 – 9.4	6.6 – 10.6
Nb	1.5 – 1.7	1.3 – 1.8	4.3 – 4.9	3.5 – 4.7
Ta	2.9 – 3.2	2.6 – 3.2	8.3 – 9.3	5.7 – 9
Ni	Balance	Balance	Balance	Balance

(b) Elements fixed

Element	Target	Actual
	Content, wt 1%	
Co	9.4 – 10.6	8.5 – 10.2
C	0.08 – 0.09	0.02 – 0.60
B	0.009 – 0.011	0.01 – 0.30
Zr	0.09 – 0.11	0.01 – 0.19

Descaled specific weight.—After being tested for 300 cycles all specimens were electrolytically descaled. Each specimen was suspended individually in molten potassium hydroxide maintained at 370° C. A dc current of 10 A at 3 V was passed through the salt bath for 5 min. The specimen was then soaked in water for 24 hr to remove any residual material from the bath. At the end of the water soak each specimen was brushed with a soft wire brush, washed with ethanol, dried, and weighed. The descaled weight loss is the original weight minus the descaled weight. The surface area of the corroded test section of each specimen was calculated from dimensions measured by a ruler. The descaled weight change was divided by this corroded area, and the results are reported as descaled specific weight change in milligrams per centimeter squared.

Metal diameter.—The diameter of each specimen was initially measured with a micrometer caliper at three places in the hot zone (fig. 1(a)). These values were averaged to obtain the initial, or noncorroded, diameter. After being tested for 300 cycles the specimens were cross sectioned at the center of the hot zone. After being

TABLE 2.—BAR NUMBERS OF STATISTICAL DESIGN EXPERIMENT SAMPLES

[Bars 25 and 55 are lost samples. Bars 50, 56, 69, and 79 do not fit the tables compositional ranges and were not used in any regression analysis. Bars 1 to 16 were Co-variation samples used in another program.]

Element level					Low Al		High Al	
					Low Ti	High Ti	Low Ti	High Ti
					Bar number			
High Cr	High Ta	High W	High Mo	High Nb		29	28	
				Low Nb				
			Low Mo	High Nb				
				Low Nb	19, 37			75
		Low W	High Mo	High Nb				
				Low Nb	63			34
			Low Mo	High Nb			72	
				Low Nb	52			
	Low Ta	High W	High Mo	High Nb				
				Low Nb		57	59	
			Low Mo	High Nb				66
				Low Nb				
		Low W	High Mo	High Nb	30			20
				Low Nb				
			Low Mo	High Nb	24, 60, 47	73		
				Low Nb			70	
Low Cr	High Ta	High W	High Mo	High Nb	23			26
				Low Nb				
			Low Mo	High Nb				
				Low Nb	17	74	21	62
		Low W	High Mo	High Nb				
				Low Nb		54	43	68
			Low Mo	High Nb	61			31, 41, 42
				Low Nb	18, 46		76	80
	Low Ta	High W	High Mo	High Nb				
				Low Nb	58			67
			Low Mo	High Nb		39		36
				Low Nb	78		27	51
		Low W	High Mo	High Nb		35, 48	44	53
				Low Nb			33, 38	45
			Low Mo	High Nb		22, 32	40, 49	64
				Low Nb	77		65	71

mounted in epoxy they were ground, polished, and etched. The final diameter of the unattacked metal was measured with a micrometer microscope at a magnification of 150. Figure 2 shows schematically a typical cross section of a corroded specimen. The diameter was measured from nonmetal-metal interface to metal-nonmetal interface, and the macrodepleted zone and the scale layer were not included. Four diameter measurements were made and averaged. This internal diameter measurement can be made with a precision of ±0.002 mm, but experience has shown that an accuracy of only ±0.020 mm can be attained in practice (ref. 2), mainly because of the irregularity of attack. The change in diameter is the difference between the initial caliper-measured diameter and the final internal metal diameter and is reported in millimeters.

Cross-sectional area of metal.—The cross-sectional areas of the specimens, after 300 cycles of testing, were measured from 6.5-magnification photographic enlargements of the polished and etched sections used for final metal diameter measurements. Because it was not possible to directly measure the initial uncorroded cross section for each specimen, three tested specimens were cut in

TABLE 3.—BAR NUMBER, NAME, AND ELEMENT LEVEL FOR COMMERCIAL ALLOYS

Element Level					Low Al		High Al	
					Low Ti	High Ti	Low Ti	High Ti
					Bar number			
High Co (>10 wt %)								
High Cr	High Ta	High W	High Mo	High Nb				
				Low Nb				
			Low Mo	High Nb				
				Low Nb				
		Low W	High Mo	High Nb				
				Low Nb				
			Low Mo	High Nb				
				Low Nb				
	Low Ta	High W	High Mo	High Nb				
				Low Nb				
			Low Mo	High Nb				
				Low Nb				
		Low W	High Mo	High Nb				
				Low Nb		(a)		
			Low Mo	High Nb				
				Low Nb				
Low Cr	High Ta	High W	High Mo	High Nb				
				Low Nb				
			Low Mo	High Nb				
				Low Nb				
		Low W	High Mo	High Nb			83, 87	
				Low Nb				
			Low Mo	High Nb				
				Low Nb				
	Low Ta	High W	High Mo	High Nb				
				Low Nb				
			Low Mo	High Nb				
				Low Nb				
		Low W	High Mo	High Nb			85	
				Low Nb			90	93
			Low Mo	High Nb				
				Low Nb			86, 94	

Element Level					Low Al		High Al	
					Low Ti	High Ti	Low Ti	High Ti
					Bar number			
Low Co (<10 wt %)								
High Cr	High Ta	High W	High Mo	High Nb				
				Low Nb				
			Low Mo	High Nb				
				Low Nb				
		Low W	High Mo	High Nb				
				Low Nb				
			Low Mo	High Nb				
				Low Nb				
	Low Ta	High W	High Mo	High Nb				
				Low Nb				
			Low Mo	High Nb				
				Low Nb				
		Low W	High Mo	High Nb				
				Low Nb				
			Low Mo	High Nb				
				Low Nb	84	89		
Low Cr	High Ta	High W	High Mo	High Nb				
				Low Nb				
			Low Mo	High Nb				
				Low Nb				
		Low W	High Mo	High Nb			81, 92	
				Low Nb			96	
			Low Mo	High Nb				
				Low Nb				
	Low Ta	High W	High Mo	High Nb				
				Low Nb				
			Low Mo	High Nb				
				Low Nb			95	
		Low W	High Mo	High Nb				
				Low Nb				
			Low Mo	High Nb				
				Low Nb				

[a]Bars 82, 88, 91, 4, 5, and 10.

TABLE 3.—Concluded.

Element	Element level, wt %	
	Low level	High level
Al	2.5–4.1	4.7–6.2
Ti	0–2.6	3.1–6.2
Co	<10	>10
Cr	4.1–10.7	12.6–18
Ta	0–4.2	5.2–8.1
W	0–5.2	6.2–7
Mo	0–2.4	2.8–6
Nb	0–2.8	3.5–4.8

Bar	Alloy
81,92	TAZ-8A
82	U710
83	XI-A
84	MAR-M 421
85	IV-E
86	M-246
87	XD-1
88,91	U700
89	IN-738
90	B-1900
93	IN-100
94	MAR-M 211
95	René 125
96	TRW-R
4	U700
5	U700
10	U700

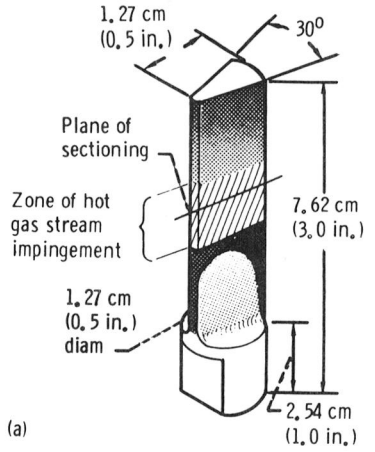

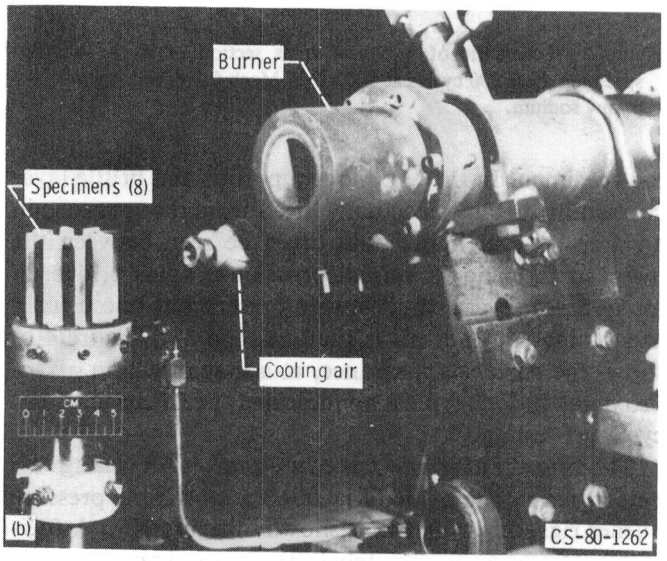

(a) Test bar.
(b) Burner rig.

Figure 1.—Hot-corrosion apparatus and test specimen.

the cool, uncorroded part and then mounted, polished, etched, and photographed. The average of the three measured areas for these sections was used as the original area for all specimens. The actual area was measured by following the unattacked metal perimeter with an electronic pen on a graphics tablet connected to a microcomputer that calculated the area. Five traces of the metal outline, as depicted in the schematic of a typical cross section in figure 2, were made and an average of the five values was used. The results are reported as loss of metal cross-sectional area in percent. These values were obtained by taking the difference between the original and tested areas and dividing by the original area.

Coil measurements.—At 15-cycle test intervals the inductance of a solenoid coil containing the test specimen as a core was measured. The coil-specimen combination mounted in the test fixture of the multifrequency inductance-capacitance-resistance (LCR) meter is shown in figure 3. The wedge shape of the coil was similar to that of the specimen but slightly larger so it could accommodate the specimen even after some scale buildup. A frequency of 10 MHz was used for all measurements. The coil inductance was measured for each of four insertions of the specimens into the coil. The average, in microhenries, is reported. Calculations, measurements, and data handling were performed on-line by a microcomputer. More detailed information on the coil measurement technique is given in reference 13.

Visual examination.—At the end of testing (300 cycles) and after descaling, each specimen was examined by the unaided eye. The specimens could be arranged in several attack-mode categories, which were defined as NC—no corrosion, CHZ—most corrosion in the hottest portion of the flame impingement zone, CCZ—most corrosion in the cooler portions of the flame impingement zone, and ML—metal lifting. Figure 4(a) shows typical profiles of these modes schematically. The schematic for the CCZ mode shows two symmetrical attack areas; however, only one area was observed in some cases, often at the top of

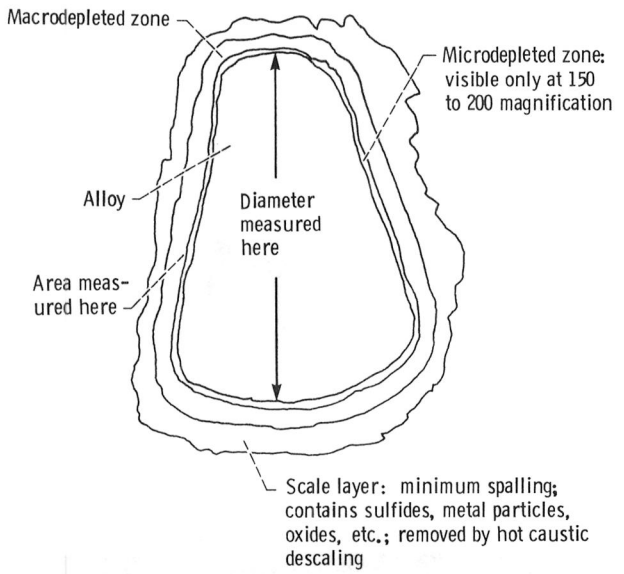

Figure 2.—Schematic of a typical cross section of wedge bar test specimen after 300 cycles at 900° C in Mach 0.3 burner rig with 0.5 ppmw sodium.

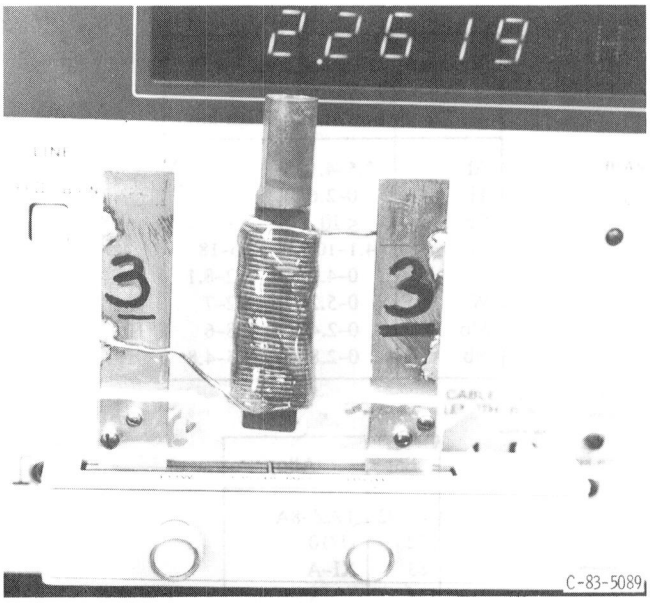

Figure 3.—Induction coil and specimen.

the specimen. In the ML mode a porous and brittle layer containing metal was actually lifted from the specimen in an arch so that light could often be seen between the metal surface and the raised corrosion-product bridge. In many cases several modes were present but one usually predominated, and this is the one reported. Figure 4(b) shows the surface appearance, at a magnification of approximately 2, of typical nondescaled specimens after 200 cycles of testing.

Corrosion testing and test conditions.—All testing was performed in one of two Mach 0.3 atmospheric pressure burner rigs, one of which is shown in figure 1(b). A fuel-to-air ratio of approximately 0.04 was used and the combustion air was preheated to 235° C. Eight specimens at a time, contained in a carousel, were rotated at 600 rpm in the flame path. The surface temperature of the specimens was measured with an optical pyrometer that had been previously calibrated against a thermocouple located inside a dummy test specimen. The specimen temperature was maintained at a nominal 900° C for 1 hr and then cooled for 3 min to about 100° C by a stream of air. This made up one corrosion test cycle. Because the heating time was 1 hr, cycles and hours can be used interchangeably. The flame was doped with 0.5 ppmw (parts by weight per million parts of combustion air) of sodium added to the combustion chamber as an aspirated water solution of sodium chloride. Jet A-1 fuel containing 0.05 to 0.07 wt % sulfur was used.

Test Results and Discussion

The experimental test results for all test samples are tabulated in appendix A.

Corrosion Test Results

Visual appearance of descaled samples.—Although visual appearance is very simple and subjective, it gives an interesting macropicture of overall attack. Table 4 gives the mode of attack deduced from visual examination of the descaled specimens after 300 cycles. This table is arranged to reflect the alloy composition by high and low levels of element content. High means the alloy contained that element in the high-level range as given in table 1, and low means in the low-level range. For example, high Al means the alloy had an aluminum content of 5.0 to 7.2 wt %, and low Al indicates an aluminum content of 1.7 to 3.3 wt %.

The results presented in table 4 indicate that only compositions with high Cr content, irrespective of the Al content, showed the NC mode of attack, and no compositions with low Cr content showed this mode. Only compositions with low Cr and high Al contents showed the ML mode. The CCZ and CHZ modes were distributed over the entire compositional range.

Figure 4(b) shows typical corrosion test bars (not descaled) after 200 cycles of testing. Flame impingement was on the narrower edge. Specimen A is typical of the CHZ mode of attack, specimen B is typical of the CCZ mode, and specimen C represents the ML mode. After 300 cycles and descaling, the contours were more prominent, but no photographs are available.

The variation of attack that occurred in the lateral direction is illustrated by photographs taken at a 6.5 magnification of the cross sections of several typical alloys (fig. 5). These sections were taken of descaled specimens at the maximum temperature zone in every case. Direct flame impingement was on the smaller end of

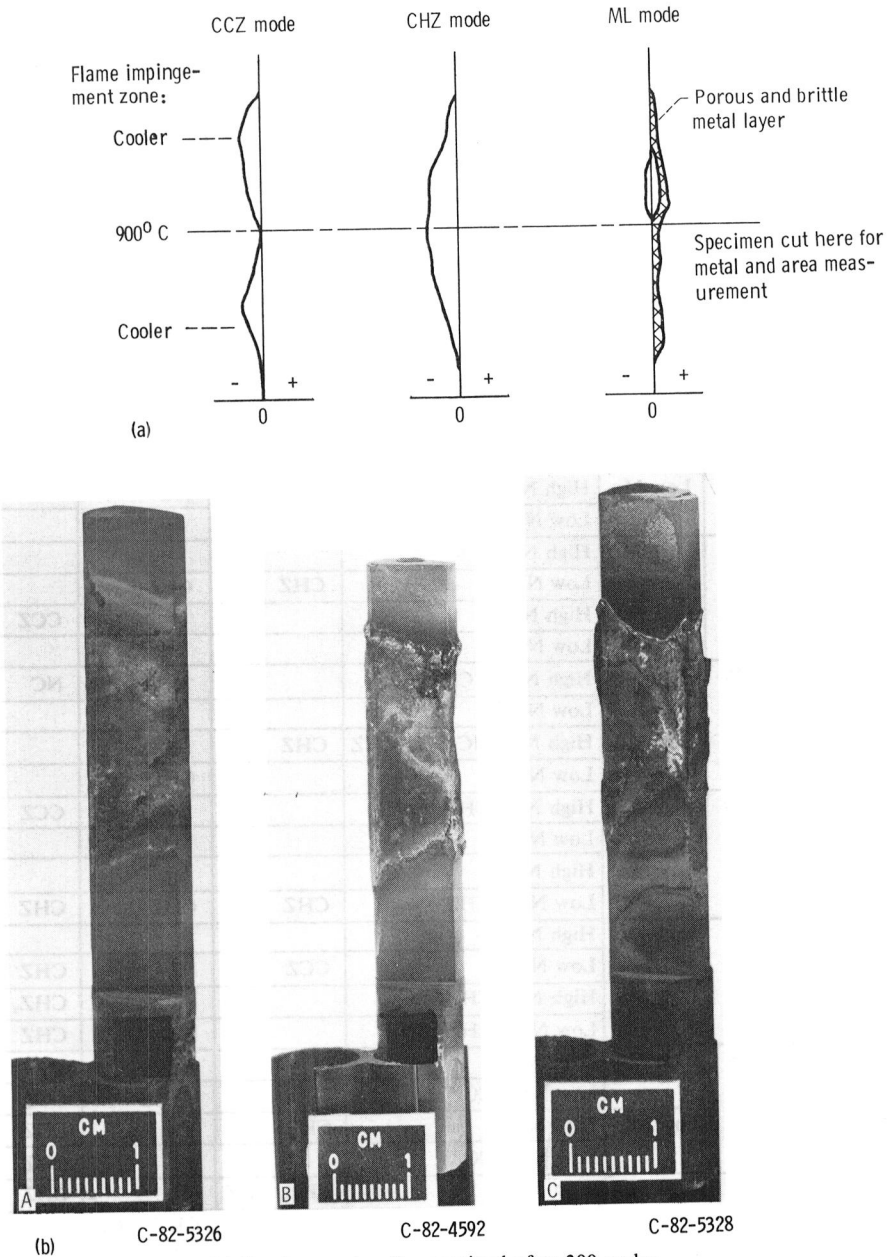

(a) Specimens visually examined after 300 cycles.

(b) Specimens photographed after 200 cycles (not descaled). Magnification, ~2.

Figure 4.—Typical appearance of corroded specimens. (+ denotes surface above original metal; - denotes corroded surface below original metal; 0 denotes original metal surface).

the wedge. An untested cross section (fig. 5(a)) is shown for comparison. Figure 5(b) illustrates an alloy with greater attack on the rear surface than on the flame impingement surface. Figure 5(c) is the reverse: this alloy shows greater attack on the flame impingement surface. Figure 5(d) shows uniform attack on all surfaces. All three corroded alloys exhibited some degree of metallic depletion zone formation, but this was not necessarily typical.

These simple visual observations give insight into the wide variety of hot-corrosion attack exhibited by various alloy compositions and the difficulties involved in measuring the extent of such attack on alloys of diverse composition tested in a high-velocity burner rig flame.

TABLE 4.—VISUAL APPEARANCE OF DESCALED TEST BARS AFTER 300 CYCLES

[NC = no corrosion detected; CHZ = most corrosion in hot zone; CCZ = most corrosion in cooler zone; ML = metal lifting]

Element level					Low Al		High Al	
					Low Ti	High Ti	Low Ti	High Ti
					Visual appearance			
High Cr	High Ta	High W	High Mo	High Nb		CCZ	CCZ	
				Low Nb				
			Low Mo	High Nb				
				Low Nb	NC, CHZ			NC
		Low W	High Mo	High Nb				
				Low Nb	CHZ			CHZ
			Low Mo	High Nb			NC	
				Low Nb	CHZ			
	Low Ta	High W	High Mo	High Nb				
				Low Nb		CHZ	CCZ	
			Low Mo	High Nb				CCZ
				Low Nb				
		Low W	High Mo	High Nb	CCZ			NC
				Low Nb				
			Low Mo	High Nb	NC, NC, CHZ	CHZ		
				Low Nb			CHZ	
Low Cr	High Ta	High W	High Mo	High Nb	CHZ			CCZ
				Low Nb				
			Low Mo	High Nb				
				Low Nb	CHZ	CHZ	CHZ	CHZ
		Low W	High Mo	High Nb				
				Low Nb		CCZ	ML	CHZ
			Low Mo	High Nb	CHZ			CHZ, ML, CHZ
				Low Nb	CHZ, CHZ		ML	CHZ
	Low Ta	High W	High Mo	High Nb				
				Low Nb	CCZ			CCZ
			Low Mo	High Nb		CHZ		CHZ
				Low Nb	CCZ		ML	CHZ
		Low W	High Mo	High Nb		CHZ, CHZ	ML	CHZ
				Low Nb			CHZ, CCZ	CCZ
			Low Mo	High Nb		CHZ, CHZ	ML, ML	CHZ
				Low Nb	CHZ		CCZ	CCZ

Descaled specific weight.—Table 5 lists the specific weight loss for each descaled specimen after 300 cycles. In general the weight loss was least for the high-Cr-content alloys and greater for the low-Cr-content alloys, with the alloys of greatest losses clustered in the area of low Cr, high Al, and high and low Ta content. Although the determination of weight loss is an analytical method, it can return deceptive results because the descaling process removes only the outermost oxide-sulfide-sulfate corrosion product layer and leaves the altered metallic corrosion-product layers. Thus the weight loss can be too little if the alloy has formed extensive depleted layers or layers with entrapped metallic constituents. This method also gives only an average measure of attack for the whole corrosion zone. It is herein assumed that the depleted or altered layers must be considered as destroyed alloy. A further disadvantage of this method is that it is destructive and can be performed only at the end of a test. If intermediate results are desired, an equivalent specimen must be available and tested. This is often expensive, and equivalent specimens may differ in physical-chemical properties.

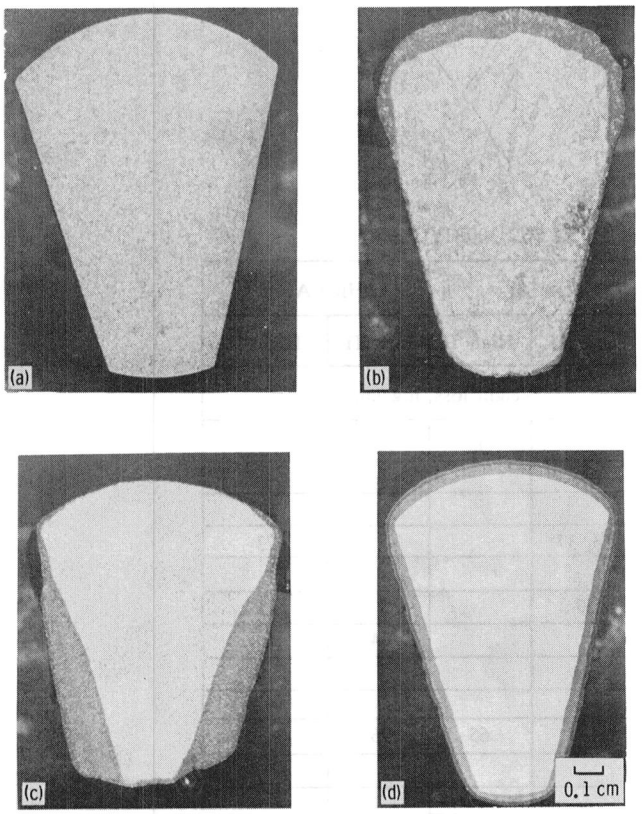

(a) Not tested.
(b) Greater attack on rear surface.
(c) Greater attack on flame impingement surface.
(d) Uniform attack.

Figure 5.—Typical test specimen cross sections after 300 cycles at 900° C in Mach 0.3 burner rig with 0.5 ppmw sodium and descaling. Magnification, 6.5. Flame impingement on narrow end of wedge.

Diameter and cross-sectional area of residual metal.—At first glance these methods might appear to be equivalent. However, they are only equivalent for circular-cross-section specimens rotating on their own axes during testing. For noncircular cross sections or samples moving through the center of the flame on other than their own axes, corrosion of some alloys can produce larger area changes than that produced by the change in diameter. For wedge-shaped samples tested in an eight-sample carousel, the area of some alloys can decrease more than the corresponding diameter change would indicate, because the corrosion is greater on the sides of the wedge. The area measurement is independent of the uniformity of corrosion, so it is the better index of corrosion resistance. Nevertheless, results of both measurements are reported. The loss of metal diameter in millimeters is given in table 6, and the percentage loss of the metal area, in table 7. Both values were determined on the same cross section, which was located at the maximum-temperature zone on the specimen. These results are more absolute measures of attack than the descaled specific weight measurements because they exclude any retained corrosion product and the depletion zone. Also, they apply only to the specified test temperature. These measurements suffer the same drawback as the specific weight loss measurements of descaled specimens in that the specimen must be destroyed to make the measurement.

In very general terms the diameter and area results led to the same compositional conclusions, and they agreed with those reached on the basis of the descaled weight loss; that is, the least corrosion occurred for high-Cr-content alloys, attack was greater for low-Cr-content alloys, and the greatest attack occurred for alloys in the compositional region of low Cr, high Al, and both high and low Ta content.

Coil measurements.—Coil measurement is a new nondestructive method being used to detect the changes in alloys exposed to corrosive conditions. It has been successfully used to study the flame corrosion of U700 alloy (refs. 13 and 15). However, it had not been applied to a wide range of alloy compositions. Inductance versus cycles of exposure data were obtained for all of the alloys studied. Figure 6 is a typical inductance curve for an alloy sample that exhibited no metal lifting, and figure 7 is typical of a sample that showed moderate metal lifting. These two types of behavior are typical of many of the alloys in this study. Metal lifting, or metal separation, is the corrosion attack mode characterized by metal particles in the corrosion product scale. These metal particles cause the inductance to decrease (fig. 7). Two other types of inductance-cycle curve shapes were also observed: straight lines, and continuous curves over the total test time. These types are largely concentrated in the high-Cr-content region. Interpreting inductance-cycle curve shapes is discussed in reference 13. It was concluded (ref. 13) that the inductance curve shape changed in unison with compositional and volume changes in the alloy induced by corrosion. Briefly, the initial large increase in inductance during the induction or incubation period of corrosion (ref. 16) is due to a change in the composition of a thin surface layer of the alloy. For no metal lifting (fig. 6) the final sharp increase starting at about 240 cycles was the onset of catastrophic corrosion and was caused by a loss of metal volume. It is defined herein that the useful hot-corrosion "life" of the alloy ends at the start of the catastrophic corrosion period. For moderate metal lifting (fig. 7) the inductance fell soon after the initial rise because metal particles in the scale made the "effective" diameter of the sample larger. Because this indicated a very rapid and destructive form of grain boundary attack, hot-corrosion life for this type of alloy has been defined as the point where metal lifting starts. The straight line and continuously curving inductance-cycle curves exhibited no inflection points, so no life values for these alloys have been determined. Because

TABLE 5.—DESCALED WEIGHT LOSS AFTER 300 CYCLES

Element level					Low Al		High Al	
					Low Ti	High Ti	Low Ti	High Ti
					Weight loss, mg/cm^2			
High Cr	High Ta	High W	High Mo	High Nb		98	119	
				Low Nb				
			Low Mo	High Nb				
				Low Nb	53, 37			73
		Low W	High Mo	High Nb				
				Low Nb	57			71
			Low Mo	High Nb			64	
				Low Nb	30			
	Low Ta	High W	High Mo	High Nb				
				Low Nb		65	96	
			Low Mo	High Nb				80
				Low Nb				
		Low W	High Mo	High Nb	71			39
				Low Nb				
			Low Mo	High Nb	47, 60, 60	48		
				Low Nb			181	
Low Cr	High Ta	High W	High Mo	High Nb	196			157
				Low Nb				
			Low Mo	High Nb				
				Low Nb	153	99	163	157
		Low W	High Mo	High Nb				
				Low Nb		86	193	187
			Low Mo	High Nb	182			88, 181, 90
				Low Nb	130, 152		346	288
	Low Ta	High W	High Mo	High Nb				
				Low Nb	189			222
			Low Mo	High Nb		114		154
				Low Nb	114		255	139
		Low W	High Mo	High Nb		114, 109	237	156
				Low Nb			352, 355	273
			Low Mo	High Nb		71, 95	296, 306	430
				Low Nb	100		298	379

TABLE 6.—INTERNAL METAL DIAMETER LOSS AFTER 300 CYCLES

Element level					Low Al		High Al	
					Low Ti	High Ti	Low Ti	High Ti
					Metal diameter loss, mm			
High Cr	High Ta	High W	High Mo	High Nb		0.258	0.131	
				Low Nb				
			Low Mo	High Nb				
				Low Nb	0.18, 0.194			0.199
		Low W	High Mo	High Nb				
				Low Nb	0.278			0.097
			Low Mo	High Nb			0.176	
				Low Nb	0.266			
	Low Ta	High W	High Mo	High Nb				
				Low Nb		0.263	0.09	
			Low Mo	High Nb				0.19
				Low Nb				
		Low W	High Mo	High Nb	0.424			0.059
				Low Nb				
			Low Mo	High Nb	0.343, 0.163, 0.179	0.403		
				Low Nb			1.449	
Low Cr	High Ta	High W	High Mo	High Nb	0.595			0.371
				Low Nb				
			Low Mo	High Nb				
				Low Nb	0.902	0.706	1.124	0.443
		Low W	High Mo	High Nb				
				Low Nb		0.772	1.429	1.021
			Low Mo	High Nb	1.485			0.967, 1.058, 1.666
				Low Nb	0.759, 0.704		3.034	2.295
	Low Ta	High W	High Mo	High Nb				
				Low Nb	1.008			1.176
			Low Mo	High Nb		0.519		0.54
				Low Nb	0.776		2.699	1.073
		Low W	High Mo	High Nb		0.833, 1.387	2.455	1.77
				Low Nb			1.585, 1.607	1.372
			Low Mo	High Nb		0.866, 0.747	2.407, 2.913	2.984
				Low Nb	0.658		1.588	2.71

TABLE 7.—LOSS OF METAL CROSS-SECTIONAL AREA AFTER 300 CYCLES

Element level					Low Al		High Al	
					Low Ti	High Ti	Low Ti	High Ti
					Percentage loss of metal cross-sectional area			
High Cr	High Ta	High W	High Mo	High Nb		1.0	2.6	
				Low Nb				
			Low Mo	High Nb				
				Low Nb	3.2, 6.4			3.0
		Low W	High Mo	High Nb				
				Low Nb	4.6			0.4
			Low Mo	High Nb			0.20	
				Low Nb	2.0			
	Low Ta	High W	High Mo	High Nb				
				Low Nb		1.2	3.9	
			Low Mo	High Nb				2.6
				Low Nb				
		Low W	High Mo	High Nb	1.6			4.2
				Low Nb				
			Low Mo	High Nb	2.2, 1.0, 1.6	5.0		
				Low Nb			26.3	
Low Cr	High Ta	High W	High Mo	High Nb	10.8			2.9
				Low Nb				
			Low Mo	High Nb				
				Low Nb	25	17.2	22	11.8
		Low W	High Mo	High Nb				
				Low Nb		10.8	24.7	16.3
			Low Mo	High Nb	29.8			12.9,13.6, 27.5
				Low Nb	11, 17.6		56.7	40.8
	Low Ta	High W	High Mo	High Nb				
				Low Nb	19.6			26
			Low Mo	High Nb		5.3		11.1
				Low Nb	19.2		29.4	20.3
		Low W	High Mo	High Nb		15.2,21	39.6	18.1
				Low Nb			31, 30.9	21.2
			Low Mo	High Nb		13.4, 8.6	35.2,54.1	46.9
				Low Nb	10.7		29.9	50.7

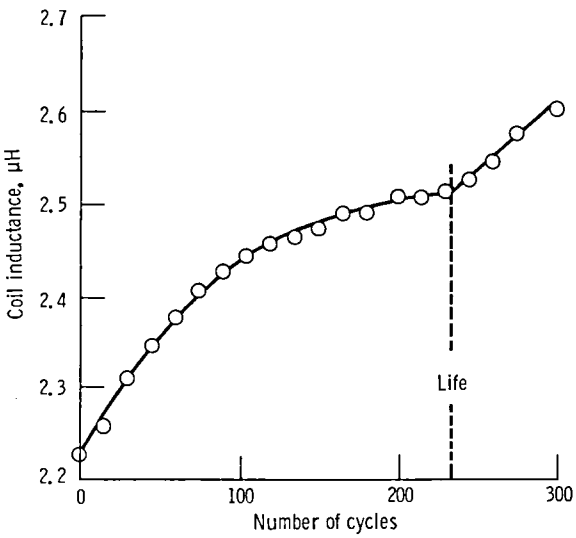

Figure 6.—Typical inductance-cycle curve of a non-metal-lifting alloy.

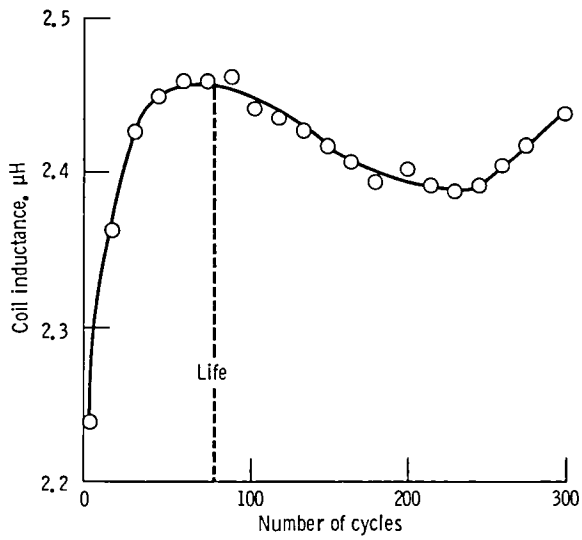

Figure 7.—Typical inductance-cycle curve of a metal-lifting alloy.

most of these alloys are high in Cr content and have good resistance to corrosion, their life has not been reached in 300 cycles of testing. Other alloys exhibiting this type of behavior may be experiencing hot-corrosion attack by some other mechanism. The life values for 27 of the original factorial design alloys that exhibited life-determining criteria are shown in figure 8 as a function of the change in inductance over the first 30 cycles. There is some scatter of the data, but it was concluded that a log-log relation exists. This was taken to imply that, by exposing the specimen for 30 cycles and determining the change in inductance of a coil-sample combination over this testing period, the life of the alloy can be estimated. For example, it can be presumed that if an alloy exhibits an inductance change of greater than 0.05 μH in 30 cycles of testing, its life will be short. In this way all very low-

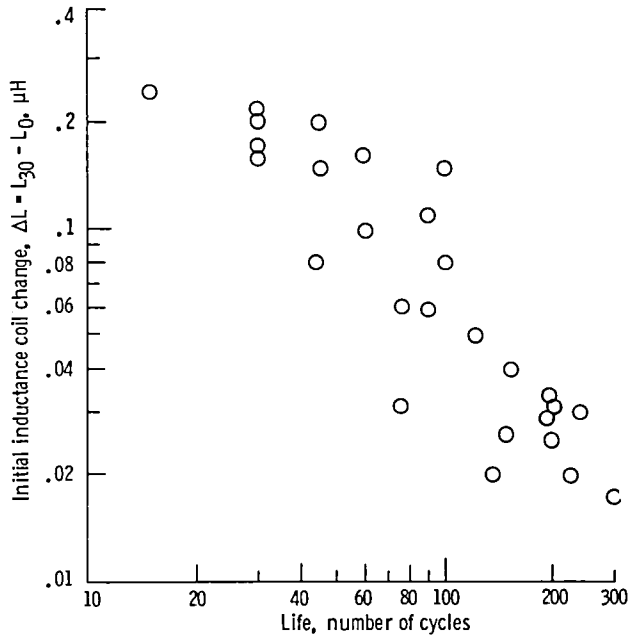

Figure 8.—Life as function of inductance change during first 30 cycles.

corrosion-resistant alloy compositions can be screened out in a short time, and testing efforts can be concentrated on the most promising alloys. The 30-cycle test time is much shorter than that required for evaluation by a destructive means. Destructive corrosion assessment, even for the least-resistant alloys, requires sufficient losses to be reliably measured and thus longer exposure and greater effort. This 30-cycle criterion is a tentative suggestion and requires further study.

In the preceding discussion the inductance change over the first 30 cycles was used to determine life. If these values are divided by 30, an approximate initial slope is defined that has the dimensions of microhenries per cycle (table 8). It has been pointed out that the high-Cr-content alloys are generally most resistant to corrosion attack as determined by destructive measurements. A scan of table 8 reveals that the high-Cr-content region contains a large population of small initial-slope values. The less resistant alloys, with low Cr content, have a large population of higher initial-slope values. Therefore it was tentatively concluded that the smaller the initial slope of the inductance curve, the more resistant the alloy is to hot-corrosion attack. An important point to make is that in 30 cycles none of the destructive methods would yield comparative corrosion resistance data because even the most corrosion susceptible alloy showed no evidence of attack after 30 cycles. It appears that the initial inductance slope from coil measurements is a very sensitive measure that can be used to predict the long-time corrosion behavior of these nickel-based alloys.

Undocumented common knowledge among aircraft turbine blade refurbishers suggests that alloys that have

TABLE 8.—INITAL SLOPE OF INDUCTANCE-CYCLE DATA

Element level					Low Al		High Al	
					Low Ti	High Ti	Low Ti	High Ti
					Inital slope, μH/cycle			
High Cr	High Ta	High W	High Mo	High Nb		0.00028	0.00035	
				Low Nb				
			Low Mo	High Nb				
				Low Nb	0.00114 0.00149			0.0007
		Low W	High Mo	High Nb				
				Low Nb	0.00167			0.00024
			Low Mo	High Nb			0.00073	
				Low Nb	0.00258			
	Low Ta	High W	High Mo	High Nb				
				Low Nb		0.00002	0.00038	
			Low Mo	High Nb				0.00017
				Low Nb				
		Low W	High Mo	High Nb	0.00064			0.0002
				Low Nb				
			Low Mo	High Nb	0.00235 .00257 .00218	0.00098		
				Low Nb			0.00115	
Low Cr	High Ta	High W	High Mo	High Nb	0.00095			0.00022
				Low Nb				
			Low Mo	High Nb				
				Low Nb	0.00115	0.00465	0.0022	0.00166
		Low W	High Mo	High Nb				
				Low Nb		0.00141	0.00192	0.0006
			Low Mo	High Nb	0.005			0.00094 .00359 .00105
				Low Nb	0.00741 .00627		0.00046	0.00174
	Low Ta	High W	High Mo	High Nb				
				Low Nb	0.00323			0.00219
			Low Mo	High Nb		0.00239		0.00192
				Low Nb	0.00644		0.00466	.00192
		Low W	High Mo	High Nb		0.00124 .00138	0.00203	0.00086
				Low Nb			0.00492 .00409	0.00272
			Low Mo	High Nb		0.00325 .00254	0.00473 .00419	0.00129
				Low Nb	0.00747		0.00121	0.00242

been more heavily attacked by hot corrosion are attracted by a permanent magnet. The magnetic attraction of most of the alloy samples, both before and after hot-corrosion attack, was tested by hanging them from a fine thread and checking for movement by passing a horseshoe magnet near the suspended sample. None of the uncorroded alloys were attracted by the magnet. After corrosion the degree of attraction was a function of the sample composition: none of the high-Cr-content alloys were attracted, the low-Cr-, low-Al-content alloys were weakly attracted, and the low-Cr-, high-Al-content alloys were strongly attracted.

From these results and the experience gained in this study, it has once again become apparent that measuring the degree of hot corrosion by a nondestructive, or even a destructive, means and the corrosion testing itself are enormously difficult. On the basis of these collective experiences a "better" hot corrosion test is suggested in appendix B.

Compositional Effects

In the previous discussion certain broad conclusions about the effects of Cr, Al, and Ti content on corrosion were drawn from a cursory scan of the individual test results. The compositional effects of these elements, based on the appropriate averages of the various test parameters, are discussed here in more detail. A simple approach for assessing the influence of the alloying elements Ta, Nb, W, and Mo on hot corrosion is given. The shortcomings of this approach are recognized; a complete statistical analysis will be the subject of a future publication. Nevertheless the results obtained by the simple analysis are sufficiently interesting to warrant discussion.

In tables 5 to 7 the test results are arranged so that the measured value of the attack parameter is placed in its respective compositional box. These tables can be divided into eight compositional sectors based only on Al, Ti, and Cr levels. For example, sector A is high Cr, low Al, and low Ti; sector B is high Cr, low Al, and high Ti; and so on as indicated in table 9. An average of the test parameters was calculated for each sector and reported in table 9. A scan of the sector averages leads to the same conclusions made previously; that is, the high-Cr compositions are more resistant than the low-Cr compositions. If one tries to narrow in on the most resistant area of the four high-Cr sectors, some ambiguity appears because not all average parameters lead to the same conclusion. For example, if area loss is compared, alloys in sector B appear to be the most resistant; but if descaled weight is used, alloys in sector A are the best. This indicates, as pointed out earlier, that not all of the parameters are of the same sensitivity or precision. Area loss is considered to be the best absolute measure of attack. For the low-Cr sectors there is no ambiguity in the conclusion arrived at from the three destructive, long-time parameters. It appears that the alloys in sectors E and F are more resistant than those in sectors G and H and that sector F contains the most resistant alloy compositions.

The short-time, initial-slope attack parameter leads to different conclusions than those reached on the basis of the absolute measure of area loss. For example, the high-Al alloys in sectors G and H are more resistant than sector E and F alloys, and sector H contains the most resistant alloys. Although the reason for the discrepancy

TABLE 9.—MEAN VALUES OF CORROSION TEST PARAMETERS AFTER 300 CYCLES FOR EACH COMPOSITIONAL SECTOR

Cr content	Corrosion test parameter	Low Al		High Al	
		Low Ti	High Ti	Low Ti	High Ti
High	Compositional sector	A	B	C	D
	Descaled weight loss, mg/cm^2	52	70	115	66
	Metal diameter loss, mm	0.253	0.308	0.461	0.136
	Metal cross-sectional area loss, percent	2.8	2.4	8.3	2.6
	Initial slope of inductance-cycle data, μH/cycle	18.3×10^{-4}	4.3×10^{-4}	6.5×10^{-4}	3.3×10^{-4}
Low	Compositional sector	E	F	G	H
	Descaled weight loss, mg/cm^2	152	98	280	207
	Metal diameter loss, mm	0.861	0.833	2.048	1.389
	Metal cross-sectional area loss, percent	18	13.1	35.4	22.9
	Initial slope of inductance-cycle data, μH/cycle	47.4×10^{-4}	24.1×10^{-4}	30.4×10^{-4}	16.5×10^{-4}

is not apparent, note that the comparisons of the initial-slope parameters are correct if the Al level is constant; that is, sector E compares properly with F, and sector G compares properly with H. This is demonstrated in figure 9, where the slope parameter averages are plotted as a function of the three respective long-time attack averages. There appears to be reasonably good correlation for two level ranges of Al content and again the high-Al-content alloys appear to be the least resistant. Note that when all initial-slope and long-time attack parameter values were plotted, correlations with Al content were not obvious. However, linear regression analysis of such plots yielded T-ratio values that were indicative of correlation even though corresponding R^2 values showed poor fit of the data to the linear model.

A detailed listing of the compositional sector correlation (table 10) shows, in a systematic way, that Cr and Ti correlations of the initial slope and most of the long-time parameters, especially the area loss, agree. But for Al the comparison is reverse to that of the area loss. This suggests that the Al content of the alloy affects the magnetic measurements and that initial-slope results should probably be compared at equal Al contents.

Cross plots of the mean long-time sector parameters of table 9 (fig. 10) seem to show a linear relation among all of the parameters. Some offset occurred between the descaled weight loss and both area and diameter loss. If measurement error was ruled out, the direction of this offset suggested that greater attack occurred away from the hottest zone where the diameter and area measurements were made. This was visually observed in many specimens and suggested that "on the average" the corrosive conditions were more severe at regions other than the 900° C peak temperature on the sample. There was also a small offset between area and diameter (rightmost plot, fig. 10). If this was not caused by measurement error, the direction of the offset (slightly greater diameter loss in relation to the area) suggested that the attack was not uniform on the cross section. This evidence supports the visual observations discussed earlier.

Furnace cyclic oxidation resistance (ref. 14) was compared with high-velocity-flame hot-corrosion resistance together with the respective oxidation products (figs. 11 (a) and (b)). The furnace data are for 1100° C; the hot-corrosion data are for 900° C. In the low-Cr-content region the hot-corrosion resistance was poorest in the high-Al-content quadrant, where the oxidation resistance was best. In the low-Cr-, low-Al-content quadrant the hot corrosion was intermediate and the oxidation resistance was poor. In the high-Cr-content region the hot-corrosion resistance was best of all, but the oxidation resistance varied depending on the Al content, from good

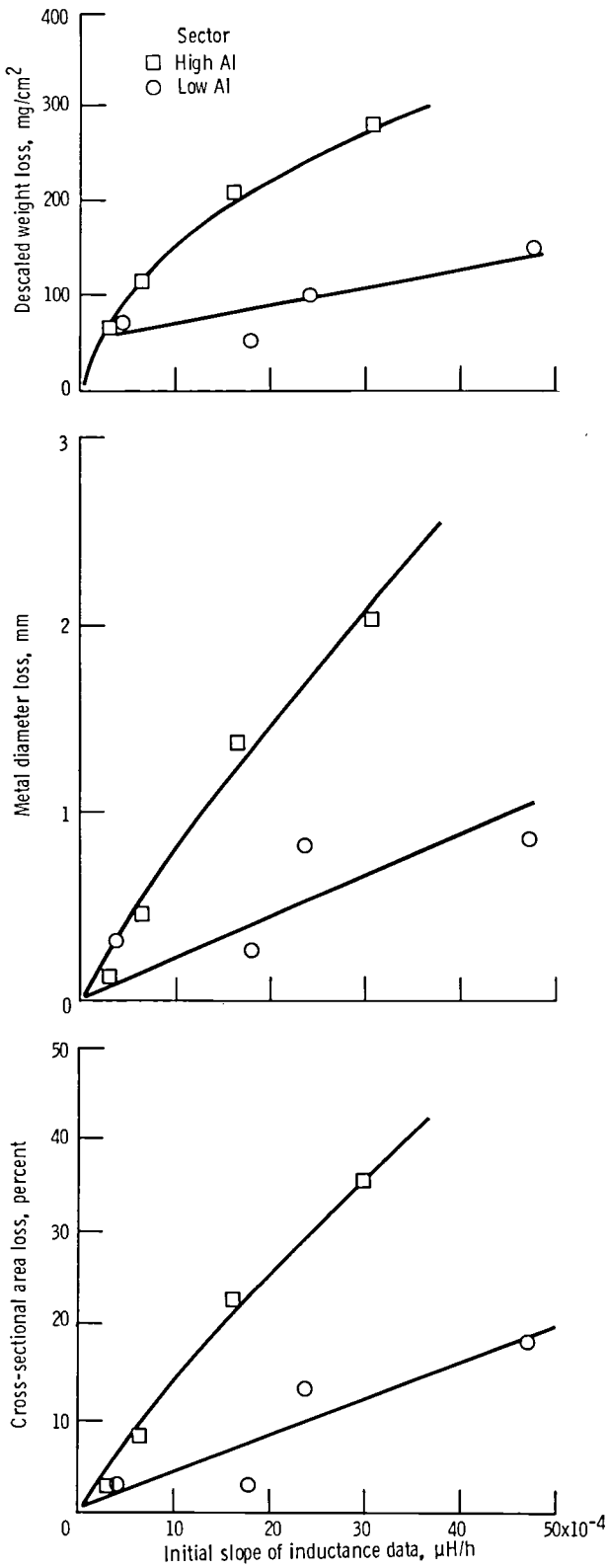

Figure 9.—Comparison of sector corrosion parameters with initial slope of inductance coil data.

TABLE 10.—CORRELATION OF COMPOSITIONAL-SECTOR MEAN CORROSION TEST PARAMETERS

[+ indicates parameter increases for sectors compared; - indicates parameter decreases for sectors compared.]

(a) Ti comparison

Corrosion test parameter	High Cr		Low Cr	
	Low Al	High Al	Low Al	High Al
	Low Ti to high Ti			
Descaled weight loss	+	-	-	-
Diameter loss	+	-	-	-
Area loss	-	-	-	-
Initial slope	-	-	-	-

(b) Al comparison

Corrosion test parameter	High Cr		Low Cr	
	Low Ti	High Ti	Low Ti	High Ti
	Low Al to high Al			
Descaled weight loss	+	-	+	+
Diameter loss	+	-	+	+
Area loss	+	+	+	+
Initial slope	-	-	-	-

(c) Cr comparison

Corrosion test parameter	Low Al		High Al	
	Low Ti	High Ti	Low Ti	High Ti
	Low Cr to high Cr			
Descaled weight loss	-	-	-	-
Diameter loss	-	-	-	-
Area loss	-	-	-	-
Initial slope	-	-	-	-

to poor. Oxidation products (fig. 11(c)) showed that the high-Al-content alloys were Al_2O_3 formers at both high and low Cr contents, and the low-Al-content alloys were NiO formers. The Al_2O_3 formers were most resistant to oxidation, but their hot-corrosion resistance varied from worst to best depending on the Cr content. Low-Al-content NiO formers exhibited poor oxidation resistance but, once again, had the best or medium hot-corrosion resistance depending on the Cr content.

Figure 12 is a dramatic, visual presentation of the effect of alloy content on hot-corrosion resistance. The photographs are arranged to correspond to sample positions from the top and the bottom rows in table 2. The alloys in figures 12(a) and (b) contain the maximum amounts of the strategic elements Cr, Ta, W, Mo, and Nb. The alloys in figures 12(c) to (e) contain the minimum amounts of these elements. This visual comparison suggests that medium hot-corrosion resistance can be achieved with alloys containing minimum amounts of the strategic elements if the Al and Ti contents are low (e.g., bar 77).

Literature information as to the effects of Al content on hot-corrosion attack is sparse. Two equations in reference 6 relate compositional data to corrosion parameters: one is the result of work by Felix and the other, by Ryan. Calculated results from both are presented in table 11 together with the loss-of-area results obtained in the present study. The compositions and temperature used for evaluation are given in the footnotes to the table. The Felix data are from flame tests at 850° C for 300 cycles using 115 ppmw sodium and 5 ppmw vanadium in the flame. Run conditions for the Ryan results are not specified. The data derived from the Felix equation agree with our results that high-Al-content alloys are less resistant than low-Al-content alloys at both high and low Cr contents. This is opposite to the findings of Ryan. However, all results agree that high Cr content is more beneficial than low Cr content. Additional information as to the effect of Al at high Cr content has been reported by Morrow, et al. (ref. 10). These results were from tests in a burner rig with 5 ppmw sea salt in which a 1-percent-sulfur diesel fuel was burned at a air-fuel ratio of 30. The specimens were cycled between 870° C and room temperature every 50 hours. The results shown in table 11, for 5 wt % Mo and no Ti, indicate that high Al content is detrimental to hot-corrosion resistance.

A preliminary effort to estimate the influence of Cr, Ta, Nb, Mo, and W content on hot-corrosion resistance was made by using a multiple linear regression model. The loss of the cross-sectional metal area was the dependent variable, and Cr, Ta, Nb, Mo, and W contents were the independent variables. The results are tabulated in table 12 and plotted in figure 13. Not unreasonable correlation coefficients were obtained together with a consistent pattern of term signs. The Cr coefficient was always negative, and the magnitude and sign of the other elements varied considerably and in an apparently systematic way as the Al-Ti compositional sectors changed. When going from high Al-Ti to low Al-Ti compositions, the magnitude increased, and the sign ultimately changed for all elements other than Cr and Mo. This may indicate that the effect of Ta, W, Mo, and Nb content on corrosion resistance may depend strongly

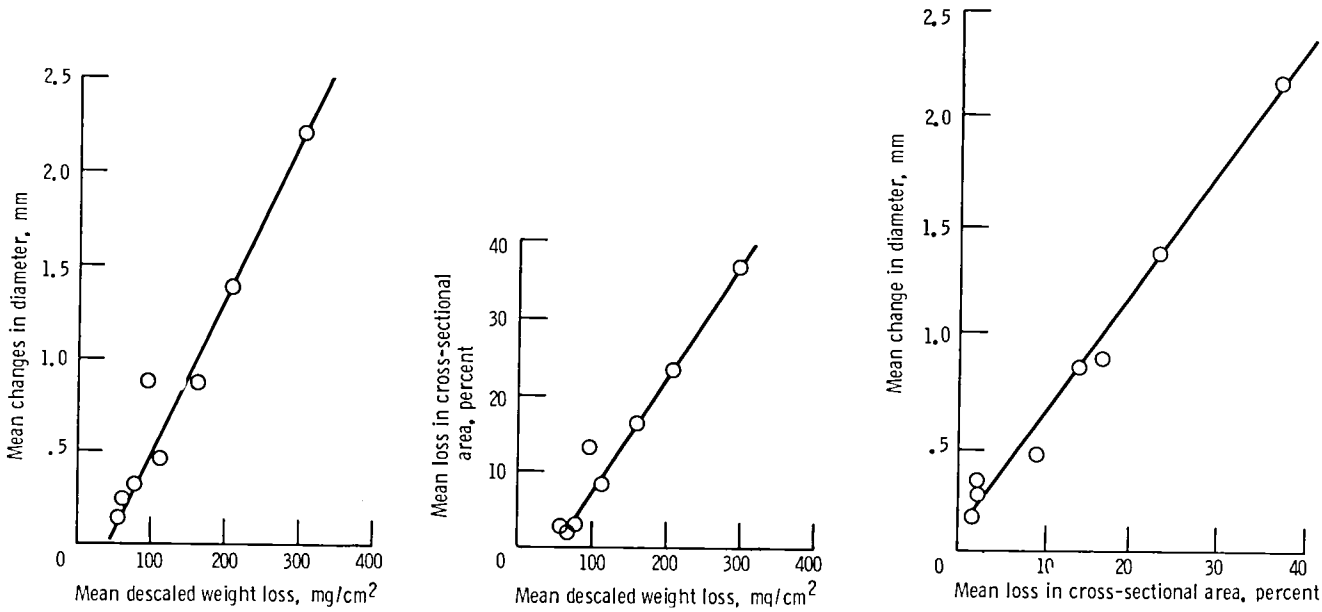

Figure 10.—Comparison of mean sector corrosion test parameters.

TABLE 11.—COMPARISON OF MEAN LOSS OF CROSS-SECTIONAL AREA CORROSION PARAMETERS WITH LITERATURE PARAMETERS

Cr content	Parameter	Al content	
		Low	High
High	Corrosion coefficient[a] (Felix, in ref. 6)	0.24	0.58
	Volume loss,[b] percent (Ryan, in ref. 6)	6.4	3
	Surface loss,[c] mils/1000 cycles (ref. 10)	12	28
	Cross-sectional area loss in 300 cycles, percent (present data)	2.6	5.5
Low	Corrosion coefficients[a] (Felix, in ref. 6)	0.32	0.78
	Volume loss,[b] percent (Ryan, in ref. 6)	17	8.1
	Cross-sectional area loss, in 300 cycles,[d] percent (present data)	15.6	29.2

[a]Calculated from wt % Al/[(wt % Ti)(wt % Cr)$^{1/2}$] where (in wt %) Ti = 2.8; high Cr = 14.1; low Cr = 7.8; high Al = 6.1; and low Al = 2.5.
[b]Calculated from $10A[5.85\times10^{-9}T^3 - 1.34\times10^{-5}T^2 + 6.33\times10^{-2}$ (wt % W) + 8.64×10^{-2}(wt % Mo) − 6.78×10^{-2}(wt % Cr) − 8.98×10^{-2} (wt % Al) + 11.28] using T = 900° C (1652° F); W = 8.6; Mo = 4.2; high Cr = 14.1; low Cr = 7.8; high Al = 6.1; low Al = 2.5.
[c]For Mo = 5; Ti = 0; low Al = 3; high Al = 6.
[d]Average values for table 9.

TABLE 12.—TERM COEFFICIENTS FOR HOT-CORROSION LINEAR REGRESSION MODEL AFTER 300 CYCLES

[Area loss as dependent variable and Cr, W, Mo, Ta, and Nb as independent variables.]

	Low Al		High Al	
	Low Ti	High Ti	Low Ti	High Ti
	Compositional sector			
	4	3	2	1
Independent variable coefficients				
Cr term	-2.6	-1.3	-3.1	-2.7
W term	.4	-.8	-2.8	-4.3
Mo term	-1.0	.7	-2.4	-6.3
Ta term	.3	.1	-1.4	-3.5
Nb term	1.0	-.1	-1.0	-3.8
Statistical data				
R^2	0.77	0.69	0.68	0.82
Standard error of estimate	5.4	5.7	12.3	7.8
Number of points	16	10	14	18

Cr content	Low Al content		High Al content	
	Low Ti content	High Ti content	Low Ti content	High Ti content
High	Low oxidation resistance 1		High oxidation resistance 2	
Low	Low oxidation resistance 3		High oxidation resistance 4	

Compositional quadrant

(a)

Cr content	Low Al content		High Al content	
	Low Ti content	High Ti content	Low Ti content	High Ti content
High	Best hot-corrosion resistance 1		2	
Low	Medium hot-corrosion resistance 3		Lowest hot-corrosion resistance 4	

(b)

Cr content	Low Al content		High Al content	
	Low Ti content	High Ti content	Low Ti content	High Ti content
High	NiO; Cr spinel; tri-rutile 1		Al_2O_3; Al spinel; tri-rutile 2	
Low	NiO; Cr spinel; tri-rutile 3		Al_2O_3; Al spinel; tri-rutile 4	

(c)

(a) Cyclic furnace oxidation at 1100° C (ref. 14).
(b) Mach 0.3 flame hot corrosion for 300 cycles at 900° C with 0.5 ppmw sodium.
(c) Oxidation products (ref. 14).

Figure 11.—Comparison of oxidation and hot-corrosion results.

on the Al–Ti content. (This interaction will be tested in the complete statistical analysis of the data and will be included in a future program.) In high Al–Ti alloys these refractory elements apparently act in a beneficial manner; in low Al–Ti alloys they range from slightly deterimental to innocuous.

Work by Ryan (reported in ref. 6) produced an analytical expression for the effects of W and Mo on the volume loss of nickel-based alloys. This equation was evaluated at 900° C to determine the effect of Al content (table 11). The results obtained from this equation (table 13) show that at both high and low levels of Cr and Al both W and Mo are detrimental to hot-corrosion resistance. This is contrary to the present results, which indicate beneficial effects of W and Mo at high Al content. Results from Morrow (ref. 10) show that (table 14) at 3 wt % Al corrosion is increased by adding 2 wt % Mo but is decreased by adding 5 and 8 wt % Mo; at higher Al contents adding Mo is beneficial at all levels of addition.

Commerical Alloy Results

The ingot compositions and test parameters for all of the commerical alloys are tabulated in appendix A (tables 18 and 19). Five specimens of U700 from two different

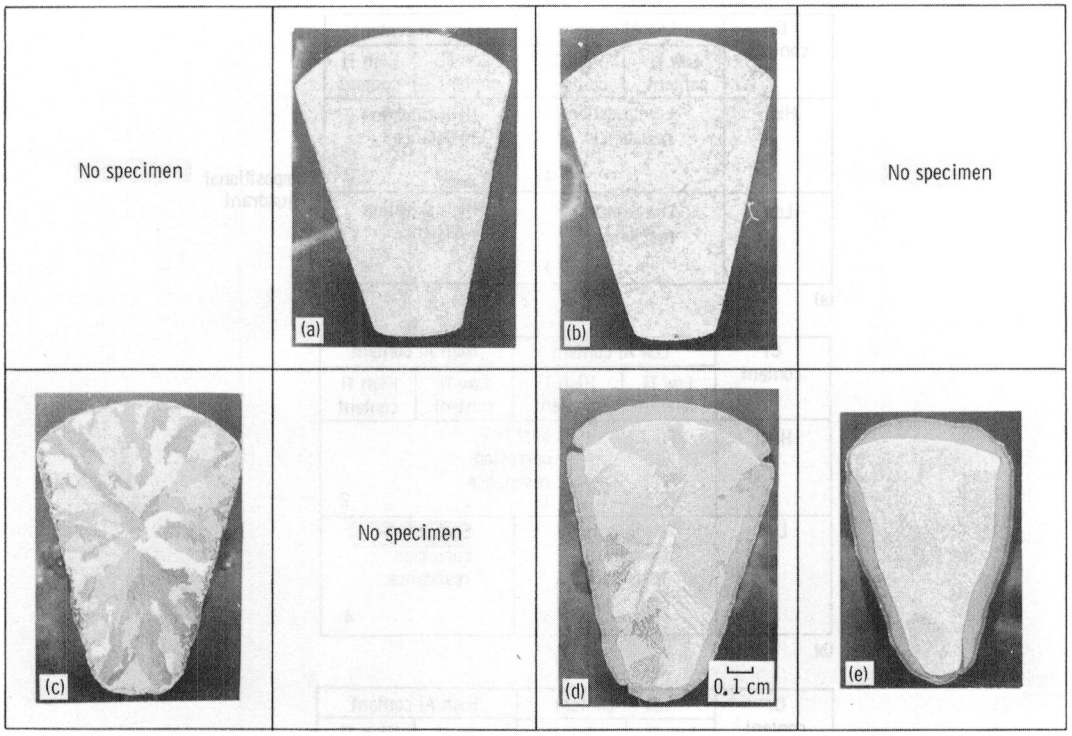

(a) Low Al, high Ti (bar 29).
(b) High Al, low Ti (bar 28).
(c) Low Al, low Ti (bar 77).
(d) High Al, low Ti (bar 65).
(e) High Al, high Ti (bar 71).

Figure 12.—Cross sections of alloys after 300 cycles in Mach 0.3 burner rig at 900° C with 0.5 ppmw sodium. Magnification, 6.5.

TABLE 13.—VOLUME LOSS FOR NICKEL-BASE ALLOYS CALCULATED FOR 900° C FROM RYAN'S EQUATION (IN REF. 6)

Element level			Low Al[d]	High Al[d]
			Volume loss, percent	
High Cr[a]	High W[b]	High Mo[c]	6.4	3.0
		Low Mo	3.7	1.8
	Low W	High Mo	3.0	1.4
		Low Mo	1.8	0.8
Low Cr	High W	High Mo	17	8.1
		Low Mo	10	4.7
	Low W	High Mo	8.1	3.8
		Low Mo	4.7	2.2

Element levels (wt %) used in calculations; equation given in table 11:
[a]High Cr = 14.1, Low Cr = 7.8.
[b]High W = 8.6, Low W = 3.5.
[c]High Mo = 4.2, Low Mo = 1.5.
[d]High Al = 6.1, Low Al = 2.5.

TABLE 14.—SURFACE LOSS FOR NICKEL-BASE ALLOYS TESTED AT 870° C FROM MORROW (REF. 10)

[Element levels in wt %; high Cr content (12.5 to 14.3 wt %); Ti content, 0.]

Nominal Mo content, wt %	Nominal Al content, wt %		
	3.0	4.5	6.0
	Surface loss, mil/1000 hr		
0	18	45	47
2	29	44	41
5	12	31	28
8	1	11	1.5

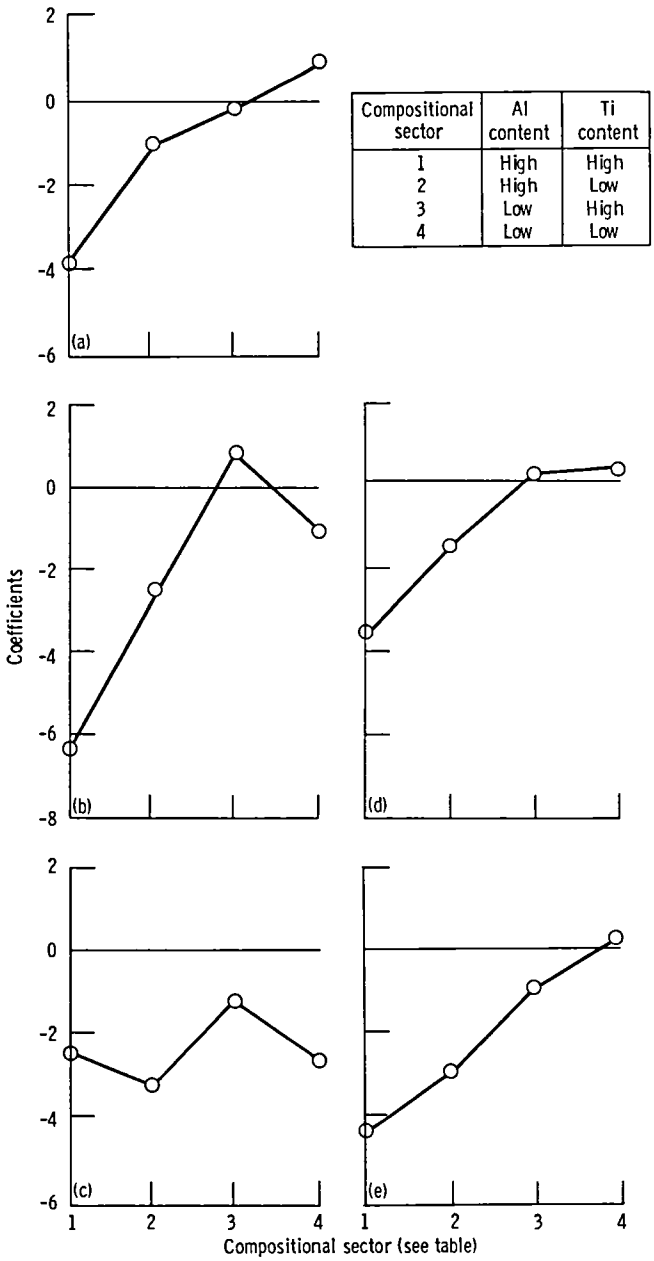

Compositional sector	Al content	Ti content
1	High	High
2	High	Low
3	Low	High
4	Low	Low

(a) Nb term. (d) Ta term.
(b) Mo term. (e) W term.
(c) Cr term.

Figure 13.—Coefficients in regression equations for multiple linear model of hot-corrosion cross-sectional area loss versus compositional area.

ingot melts and two specimens of TAZ-8A from different ingot melts were tested. The testing conditions were the same as those used for the factorial design alloys. Table 15 is a tabulation of the measured percentage of area loss and that calculated from the

TABLE 15.—CALCULATED AND MEASURED CROSS-SECTIONAL AREA LOSS AFTER 300 CYCLES FOR COMMERCIAL ALLOY COMPOSITIONS

Bar	Alloy	Al content	Ti content	Compositional sector	Calculated area loss, percent	Measured area loss, percent
81	TAZ-8A	High	Low	2	36.2	38.5
82	U710	Low	High	3	2.6	1.9
83	XI-A	High	Low	2	37.6	43.5
84	MAR-M 421	Low		4	-11	6.2
85	IV-E	High		2	38.5	59.8
86	MAR-M 246	High		2	52.8	47.6
87	XD-1	High		2	38.4	52
88	U700	Low	High	3	8.7	27.9
89	IN-738	Low	High	3	2.9	.7
90	B-1900	High	Low	2	43	46.7
91	U700	Low	High	3	8.7	16.7
92	TAZ-8A	High	Low	2	30	41
93	IN-100		High	1	68.7	54.9
94	MAR-M 211		Low	2	38.9	37
95	René 125		Low	2	31.9	26.8
96	TRW-R		Low	2	36.6	30
4	U700	Low	High	3	9.3	12.7
5	U700	Low	High	3	8.7	10
10	U700	Low	High	3	9.3	13.4

Compositional sector	Regression equation used to calculate area loss from factorial design alloys
1	111.9 - 2.7Cr - 4.3W - 6.3Mo - 3.5Ta - 3.8Nb
2	88.8 - 3.1Cr - 2.8W - 2.4Mo - 1.4Ta - 1.0Nb
3	24.8 - 1.3Cr - 0.8W + 0.7Mo + .1Ta - 0.1Nb
4	34.4 - 2.6Cr + 0.4W - 1.0Mo + 0.3Ta + 1.0Nb

multiple linear regression equations derived previously. These equations were determined from multiple linear regression analysis by using the measured area loss as the dependent variable and Cr, W, Mo, Ta, and Nb content as the independent variables for the factorial design alloy test parameters for each of the four Al-Ti compositional areas. These regression equation coefficients are given in table 12 and are repeated in the footnote of table 15 along with the constant term. The appropriate equation for the Al-Ti level of the commercial alloy was chosen for the calculation. The calculated area loss for alloy MAR-M 421 is grossly out of line probably because the large Cr content of this alloy was far outside the range of the derived regression equation. Also, the measured values for the five U700 alloys vary over a wide range, but all of the calculated values are nearly the same. The calculated

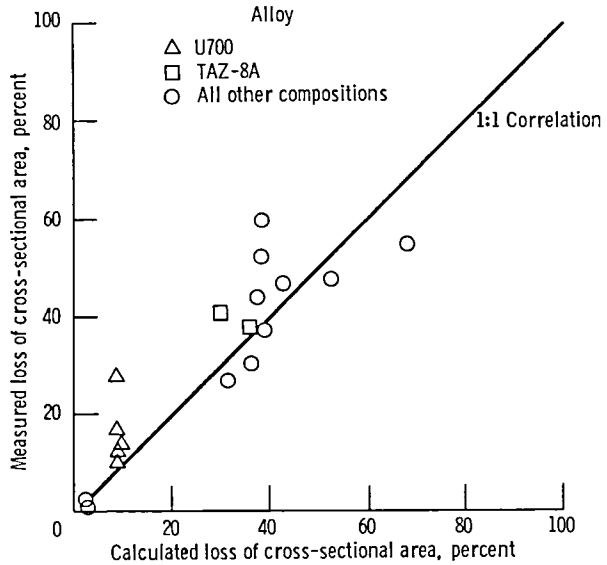

Figure 14.—Calculated and measured loss of cross-sectional area after 300 cycles for commerical alloy compositions.

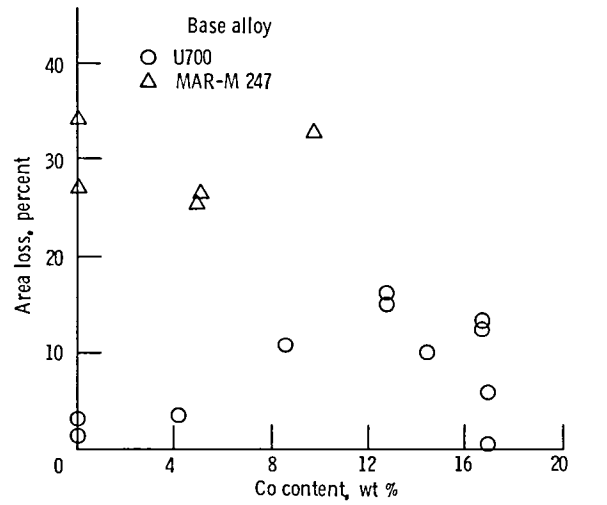

Figure 15.—Percentage of cross-sectional area loss as function of Co content for U700 and MAR-M247 alloys after 300 cycles. (Co substituted for Ni.)

values are similar because both ingots were closely alike in composition and because the Al and Ti levels were in the same range. The reason for the spread in the measured values is not obvious at this time.

The measured and calculated results, with the exception of those for MAR-M 421, are plotted in figure 14. Even with the simple linear regression equations used, where a term for Co and interaction terms were neglected, the data points were clustered close to the 1:1 correlation line. This is encouraging and suggests that even better schemes for predicting the effect of composition on corrosion should evolve from a complete statistical analysis.

Co Substitution for Ni in U700 and MAR-M 247

The ingot compositions and test parameters for these alloys are tabulated in appendix A (tables 20 to 23). The percentage of cross-sectional area loss after 300 cycles of testing as a function of the Co content (fig. 15) shows that Co content had little effect on the corrosion resistance of MAR-M 247. For U700, however, a noticeable change in corrosion attack occurred with Co content. Reducing the Co content to near zero increased the corrosion resistance, and levels near 12 wt % seemed to yield the most attack susceptibility.

Conclusions

In investigating the effects of Cr, Al, Ti, Mo, Ta, Nb, and W content on hot corrosion of nickel-base alloys, the following conclusions were drawn:

1. The best destructive method of assessing absolute corrosion was the loss of cross-sectional area of the metal. It is specific for a chosen area representative of a specific test temperature and is independent of nonuniform circumferential attack.

2. The nondestructive initial-slope measurements of the induction coil method correlated well with long-term corrosion resistance for nearly constant Al levels in two ranges. Also, the initial slope appeared to have utility in some screening life determinations for most, but not all, alloy compositions.

3. Alloys with Cr content greater than 12 wt % were most resistant to hot-corrosion attack. However, some lower-Cr-content alloys (<10 wt %) were reasonably resistant provided that the Al content was less than 2.5 wt % and the Ti content was less than 4 wt %.

4. On the basis of some preliminary and crude analyses the effects of Ta, Mo, W, and Nb content on corrosion resistance could not be well defined. They may be highly dependent on the presence of other elements such as Al. These elements appeared to be beneficial at low Al content but to range from slightly detrimental to innocuous at higher Al concentrations.

5. The calculated hot-corrosion resistance of several commercial alloys was in reasonable agreement with measured values within the compositional range of elements used in the model equations.

6. The results of this study have clarified the role played by certain test parameters and suggest a "better" hot-corrosion test procedure. It is based mainly on differences in specimen geometry, position of a single specimen in the flame, and specimen-to-nozzle distance. The objective was more uniform test conditions.

National Aeronautics and Space Administration
Lewis Research Center
Cleveland, Ohio, March 20, 1984

Appendix A
Ingot Analysis and Corrosion Parameters of Factorial Design and Commercial Alloys

TABLE 16.—BAR NUMBERS AND COMPOSITIONS OF FACTORIAL DESIGN ALLOYS

Bar	Composition, wt %									
	Cr	Al	Ti	W	Mo	Ta	Nb	Co	Zr	B
75	13.5	7.1	4	8.9	1.3	6.2	1.8	9	0.07	0.02
34	12.6	6.9	4.3	4.3	4.5	7	1.5	9	.06	.01
66	14.5	7	4.7	4.7	1.5	2.6	4.3	9.2	.09	
20	13.3	7.2	4.8	4	5	2.6	3.8	9.3	.09	
26	6.1	5.7	3.8	7.1	3.4	8	3.8	9.3	.08	
62	6.9	6.1	4.2	8.8	1.3	8.1	1.5	9.4	.10	
68	6.8	6.4	4.1	4.3	4.1	8.2	1.5	9.5	.10	
31	6.4	6.1	4.1	4.1	1.5	8.6	3.9	9.4	.08	
42	6.4	6.1	4.1	4.1	1.5	8.6	3.9	9.4	.08	
41	9.4	5.5	4	3.1	1.4	7	4.1	8.8	.09	
80	7	6.2	4.3	3.6	1.5	8.6	1.5	9.6	.06	
67	7.6	6.6	4.2	6.6	4.1	3.2	1.5	9.7	.09	
36	7.1	5.4	4.4	10.3	1.6	3.2	4.2	9.5	.08	
51	8.1	6.5	4.5	6.9	1.6	2.9	1.7	9.8	.09	
53	7.9	6.4	4.4	3.6	4.8	2.7	4.5	9.8	.10	
45	8.2	5	4.5	3.4	4.8	2.9	1.7	9.9	.10	
64	7.7	6.4	4.7	3.7	1.6	3.1	4.7	9.9	.11	
71	8.9	6.5	4.9	3.4	1.8	2.9	1.7	10	.10	
28	13.5	6.6	1.4	8.9	3.8	6.4	3.8	8.7	.01	.02
72	13	6.8	1.3	4.6	1.5	7.1	4	9.1	.08	.01
59	15.1	7.2	1.3	10.6	4.1	2.8	1.5	9	.06	.02
70	15.6	6.9	1.7	3.3	1.7	3	1.8	9.7	.10	.01
43	7.4	5.6	1.4	4.1	4.1	8.8	1.5	9.5	.09	.01
76	8.1	6	1.5	3.1	1.5	9	1.6	9.7	.09	.01
27	7.9	6.1	1.5	8.7	1.4	2.9	1.4	9.8	.16	.02
44	8.4		1.5	3.3	4.7	2.9	4.1	10	.11	.01
33	8.8		1.6	3.4	4.8	3.1	1.7	9.9	.09	.30
38	8.8			3.4	4.8	3.1	1.7	9.9	.09	.30
40	8.7	5.8		3.3	1.7	3.2	4.4	10	.11	.20
49	8.7	5.8		3.3	1.7	3.2	4.4	10	.11	.20
65	9.4	7	2	3.5	1.6	2.7	1.7	10.2	.13	.01
21	7.4	5.7	1.4	9.3	1.3	7.7	1.4	9.4	.10	.02
29	13.2	2.3	3.1	10.1	3.8	5.7	3.5	8.5	.08	.10
57	14	2.3	4.3	9.3	4	1.6	1.5	8.8	.08	.02
73	13.8	2.3	4.9	3.8	1.7	3	1.8	9.2	.09	.01
74	6.6	2.1	3.8	7.6	1.3	8.2	1.3	9	.08	.02
54	7	2.1	3.9	3	4	8.8	1.4	9.2	.08	.01
39	6.9	2.2	3.9	8.1	1.4	2.9	4	9.2	.09	
35	7.6		4.3	2.3	4.4	3	4.5	9.6	.19	
48	7.6		4.3	2.3	4.4	3	4.5	9.6	.19	
22	8.3		4.7	3.1	1.6	3.1	3.4	9	.09	
32	8.3		4.7	3.1	1.6	3.1	3.4	9	.09	
19	13.8		1.3	9.1	1.2	6.9	1.3	8.6	.07	
37	13.8		1.3	9.1	1.2	6.9	1.3	8.6	.07	
63	13.1	2.1	1.3	3.1	4.1	7	1.5	9.0	.08	
52	13.3	2.3	1.4	3.1	1.5	7.3	1.5	9.1	.01	
30	14.4	2.1	1.4	3	4.4	3	4.5	9.1	.10	
47	14.8	2.2	1.5	3	1.6	3.1	4.4	9.4	.08	
60	14.3	2.2	1.5	3.1	1.6	2.9	4.4	9.3	.09	
24	14.3	2.2	1.5	3.1	1.6	2.9	4.4	9.3	.09	
23	8.2	3.3	1.3	9	3.6	7.1	3.7	9	.06	.02
17	9.0	1.7	1.4	7.9	1.4	8.6	1.5	9.4	.09	.02
61	7.7	2.2	1.3	3.8	1.5	7.6	3.9	9.4	.06	.01
18	8	2.3	1.4	2.9	1.3	9	1.6	9.6	.09	.01
46	8	2.3	1.4	2.9	1.3	9	1.6	9.5	.09	.01
58	7.3	2.2	1.3	8.2	4	3.1	1.4	9.3	.08	.02
78	7.9	2	1.5	8	1.4	3	1.4	9.4	.08	.01
77	9.2	2	1.6	2.9	1.5	3.2	1.5	10	.08	
50	13.5	4.3	3.5	5.9	0	.1	3.2	9.5	.09	
56	13.9	3.9	3.4	5.3	0	.1	3.2	9.6	.09	
69	16	3.5	3.5	.2	5	0	0	14	.09	.02
79	8.8	4.9	1.9	10.1	0	.1	1	9.9	.11	.01

TABLE 17.—BAR NUMBERS AND CORROSION PARAMETERS AFTER 300 CYCLES FOR FACTORIAL DESIGN ALLOYS

Bar	Diameter loss, mm	Weight loss, mg/cm^2	Initial slope, μH/cycle	Area loss, percent
75	0.199	73	0.0007	3.0
34	.097	71	.00024	.4
66	.19	80	.00017	2.6
20	.059	39	.0002	4.2
26	.371	157	.00022	2.9
62	.443	157	.00166	11.8
68	1.021	187	.0006	16.3
31	.967	88	.00094	12.9
42	1.666	181	.00359	27.5
41	1.058	90	.00105	13.6
80	2.295	288	.00174	40.8
67	1.176	222	.00219	26
36	.54	154	.00192	11.1
51	1.073	139	.00192	20.3
53	1.77	156	.00086	18.1
45	1.372	273	.00272	21.2
64	2.984	430	.00129	46.9
71	2.710	379	.00242	50.7
28	.131	119	.00035	2.6
72	.176	64	.00073	.2
59	.09	96	.00038	3.9
70	1.449	181	.00115	26.3
43	1.429	193	.00192	24.7
76	3.034	346	.00046	56.7
27	2.699	255	.00466	29.4
44	2.455	237	.00203	39.6
33	1.585	355	.00409	31
38	1.607	352	.00492	30.9
40	2.407	306	.00419	35.2
49	2.913	296	.00473	54.1
65	1.588	298	.00121	29.9
21	1.124	163	.0022	22
29	.258	98	.00028	1.0
57	.263	65	.00002	1.2
73	.403	48	.00098	5.0
74	.706	99	.00465	17.2
54	.772	86	.00141	10.8
39	.519	114	.00239	5.3
35	.833	114	.00138	15.2
48	1.387	109	.00124	21
22	.747	71	.00254	8.6
32	.866	95	.00325	13.4
19	.194	53	.00114	6.4
37	.18	37	.00149	3.2
63	.278	57	.00167	4.6
52	.266	30	.00258	2
30	.424	71	.00064	1.6
47	.343	47	.00235	2.2
60	.163	60	.00257	1.0
24	.179	60	.00218	1.6
23	.595	196	.00095	10.8
17	.902	153	.00115	25
61	1.485	182	.005	29.8
18	.704	130	.00627	17.6
46	.759	152	.00741	11
58	1.008	189	.00323	19.6
78	.776	114	.00644	19.2
77	.658	100	.00747	10.7
50	.371	76	.00239	4.1
56	.235	67	.00163	5.4
69	1.352	224	.00488	22.6
79	1.663	223	.00571	30.6

TABLE 18.—BAR NUMBERS AND COMPOSITIONS FOR COMMERCIAL ALLOYS

Bar	Alloy	Composition wt %									
		Cr	Al	Ti	W	Mo	Ta	Nb	Co	Zr	B
81	TAZ-8A	6.1	5.8	0	4	3.9	8.1	1.8	0	0.57	0.005
82	U710	17.9	2.5	5	1.3	3	0	0	14	0	.012
83	XI-A	4.5	4.8	.9	5.2	4.5	5.2	4.6	10.1	.10	.01
84	MAR-M 421	18	4.1	1.8	3.5	1.7	0	1.9	9.9	.10	.02
85	IV-E	7.1	4.9	1	3.7	3.5	3.9	4.1	10.1	.11	.01
86	MAR-M 246	10.7	5.1	1.8	0	0	2	0	11.3	.01	.01
87	XD-1	4.1	5.9	.9	5.2	4.6	5.2	4.8	10.3	.11	.01
88	U700	14.6	4.1	3.3	0	4.1	0	0	14.5	.01	.013
89	IN-738	16	3.5	3.5	3	1.7	1.7	.9	8.4	.09	.01
90	B-1900	8.2	6.1	.1	0	6	4.2	.1	10	.09	.016
91	U700	14.6	4.1	3.3	0	4.1	0	0	14.5	.01	.013
92	TAZ-8A	5.9	6.2	0	6.2	3.9		2.5	0	.96	.004
93	IN-100	9	5.8	4.8	0	3		0	15.6	.07	.015
94	MAR-M 211	8.9	5	2	4.9	2.4		2.8	10.2	.03	.018
95	René 125	8.9	4.7	2.6	7	1.9	3.7	0	9.9	.07	.01
96	TRW-R	8.1	5.3	.8	4	2.8	6.3	.3	8	.12	.014
4	U700	14.8	3.9	3.1	0	5.4	0	0	16.8	.02	----
5	U700	14.6	4.1	3.3	0	4.1	0	0	14.5	.01	.013
10	U700	14.8	3.9	3.1	0	5.4	0	0	16.8	.02	----

TABLE 19.—BAR NUMBERS AND CORROSION PARAMETERS AFTER 300 CYCLES FOR COMMERCIAL ALLOYS

Bar	Alloy	Diameter loss, mm	Weight loss, mg/cm^2	Initial slope, μH/cycles	Area loss, percent
81	TAZ-8A	1.964	177	0.00247	38.5
82	U710	.451	86	.00223	1.9
83	XI-A	2.288	391	.00389	43.5
84	MAR-M 421	.641	139	.0031	6.2
85	IV-E	3.833	233	.0058	59.8
86	MAR-M 246	2.406	235	.0038	47.6
87	XD-1	3.549	744	.0052	52
88	U700	1.719	347	.0050	27.9
89	IN-738	.326	94	.0019	.7
90	B-1900	2.485	330	.0028	46.7
91	U700	1.103	390	.0083	16.7
92	TAZ-8A	2.244	283	.0034	41
93	IN-100	3.247	1151	.0072	54.9
94	MAR-M 211	2.021	631	.0062	37
95	René 125	1.663	383	.0056	26.8
96	TRW-R	1.68	327	.0050	30
4	U700	.705	226	.0057	12.7
5	U700	.628	214	.0037	10
10	U700	1.145	243	.0048	13.4

TABLE 20.—BAR NUMBERS AND COMPOSITIONS FOR U700 WITH Co SUBSTITUTED FOR Ni

[No W, Ta, or Nb content.]

Bar	Composition, wt %						
	Cr	Al	Ti	Mo	Co	Zr	B
1	15.1	4.1	3.5	5.0	0.1	0.04	0.03
2	14.9	4.1	3.6	5.0	17.0	.04	.03
3	14.9	4.1	3.6	5.0	17.0	.4	.03
4	14.8	3.9	3.1	5.4	16.8	.02	---
5	14.6	4.1	3.3	4.1	14.5	.01	.01
7	15.1	4.1	3.5	5.0	0.1	.04	.03
10	14.8	3.9	3.1	5.4	16.8	.2	---
12	15.1	4.1	3.6	4.9	4.3	.04	.02
13	14.7	↓	3.6	5.0	12.8	↓	↓
15	15	↓	3.5	5.1	8.6	↓	↓
16	14.7	↓	3.6	5	12.8	↓	↓

TABLE 21.—BAR NUMBERS AND CORROSION PARAMETERS AFTER 300 CYCLES FOR U700 WITH Co SUBSTITUTED FOR Ni

Bar	Diameter loss, mm	Weight loss, mg/cm^2	Initial slope, μH/cycle	Area loss, percent
1	0.139	30	0.00039	3.1
2	.695	63	.0033	6.0
3	.053	56	.0033	.4
4	.705	226	.0057	12.7
5	.628	214	.0037	10.0
7	.358	52	.00026	1.5
10	1.145	243	.0048	13.4
12	.358	108	.0002	3.6
13	1.604	137	.0016	15.1
15	.718	207	.00056	10.8
16	1.297	160	.0021	16.2

TABLE 22.—BAR NUMBERS AND COMPOSITIONS FOR MAR-M 247 WITH Co SUBSTITUTED FOR Ni

[No Nb content.]

Bar	Composition, wt %								
	Cr	Al	Ti	W	Mo	Ta	Co	Zr	B
6	8.4	5.5	1.0	9.8	0.7	3.0	9.8	0.04	0.01
8	8.5	5.4	.9	10.5	.7	3.2	5.0	.07	.02
9	8.4	5.1	1.0	10.2	.6	3.9	.1	.06	.01
11	8.5	5.4	.9	10.5	.7	3.2	5.0	.07	.02
14	8.4	5.1	1.0	10.2	.6	3.9	.1	.06	.01

TABLE 23.—BAR NUMBERS AND CORROSION PARAMETERS AFTER 300 CYCLES FOR MAR-M 247 WITH Co SUBSTITUTED FOR Ni

Bar	Diameter loss, mm	Weight loss, mg/cm^2	Initial slope, μH/cycle	Area loss, percent
6	2.064	269	0.0057	32.7
8	1.628	200	.0033	25.6
9	1.339	339	.00063	34.1
11	1.654	226	.0035	26.0
14	1.576	352	.00091	26.8

Appendix B
Proposed Test Procedure

During the course of much hot-corrosion testing, I have observed many nonuniform and complex interactions of doped flames with alloys tested in this laboratory's standard apparatus. This apparatus uses eight wedge-shaped specimens rotated in a carousel so that the specimens are rotated off axis and the distance of the nozzle to the specimens is 2.5 to 5 cm (1 to 2 in.) at closest approach (fig. 1). The wedge shape of the specimens makes it very difficult to assess metal loss either destructively or nondestructively. Rotating off its own axis means a specimen is exposed to varying conditions, especially temperature, in every revolution. Also, the specimens are subjected to large vertical temperature gradients and thus different corrosion environments. Furthermore the area on which the flame impinges can vary with time because mechanical disturbances in the burner may deflect the flame. The farther the nozzle is from the specimen, the more the flame moves when a disturbance is induced by warpage, carbon buildup, salt deposition, or corrosion of burner parts.

An attempt to minimize these drawbacks suggests the following changes: change the test specimen geometry, decrease nozzle-to-specimen distance, and rotate the specimen on its own long axis (fig. 16(a)). The cylindrical specimen is rotated on its own long axis so as to more evenly expose it to the flame. The center test section is only 1.27 cm (1/2 in.) long so that a 2.54-cm (1-in.) diameter flame will heat it more uniformly. The ends of the specimen are reduced in diameter to decrease heat loss from the test section and thus make the test section temperature more uniform. This geometry is easy to machine from a 1.27-cm (1/2-in.) diameter casting at a reasonable cost. With the nozzle-to-specimen distance reduced to 1.27 to 2.54 cm (1/2 to 1 in.), for a 2.54-cm (1-in.) diameter burner nozzle, the flame impingement will be more uniform, and the leverage less. Thus even when the flame changes position slightly, the same area of the specimen is always subjected to corrosion over the total test period. A two-color optical pyrometer with a 0.254-cm (0.1-in.) diameter target area or less is suggested for surface temperature measurement and a control signal. A better temperature measurement would be obtained if a small (0.00254 cm; 10 mil) diameter hole were drilled up from the bottom near the edge of the test section and a small-diameter thermocouple inserted. However, this has several serious drawbacks for long-time testing: a slipring assembly is needed and these are both expensive and short lived; expensive machining is required to produce the hole; small-diameter thermocouples have short lives; and a hole sufficiently close to the surface would be rapidly corroded into for almost all corrosion rates.

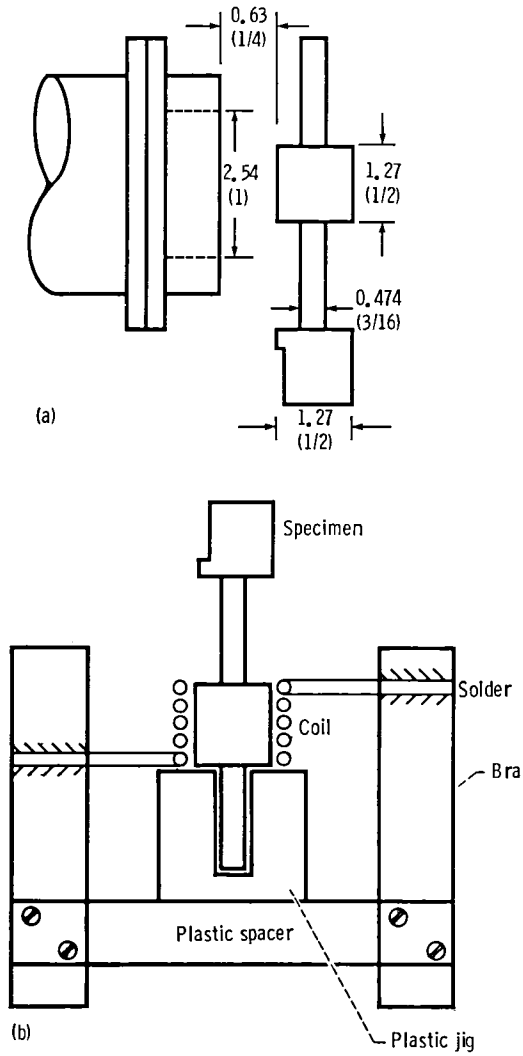

(a) Specimen and burner geometry.
(b) Coil design.

Figure 16.—Suggested specimen geometry and coil design.

The coil method for assessing attack (fig. 16(b)) is compatible with the suggested geometry of the specimen. The test section is 1.27 cm in diam by 1.27 cm long (1/2 in. by 1/2 in.), so measurement of a coil only 1.27 cm (1/2 in.) long will be over only the nearly isothermally corroded area. Even if destructive methods were used to assess the degree of attack, the measurement would be improved because of a more uniform test section

exposure. This arrangement has not been tried but will be used in the near future to study the hot corrosion of additional nickel-base alloys. It is anticipated that it will produce better results with less scatter.

References

1. Kirman, I.; et al., eds.: Behavior of High Temperature Alloys in Aggressive Environments. The Metals Society (London), 1980.
2. Deadmore, D. L.; and Lowell, C. E.: Effects of Impurities in Coal-Derived Liquids on Accelerated Hot Corrosion of Superalloys. DOE/NASA/2593-79/13, NASA TM-81384, 1980.
3. Lowell, C. E.; Sidik, S. M.; and Deadmore, D. L.: High Temperature Alkali Corrosion in High Velocity Gases. DOE/NASA/2593-28, NASA TM-82591, 1981.
4. Lowell, C. E.; et al.: The Effects of Trace Impurities in Coal-Derived Liquid Fuels on Deposition and Accelerated High Temperature Corrosion of Cast Superalloys. DOE/NASA/2593-22, NASA TM-81678, 1981.
5. Rapp, R. A., ed.: High Temperature Corrosion. National Association of Corrosion Engineers, 1983.
6. Stringer, J.: Hot Corrosion of High-Temperature Alloys, Annu. Rev. Mater. Sci., vol. 7, 1977, pp. 477-509.
7. Goebel, J. A.; Pettit, F. S.; and Goward, G. W.: Mechanisms for the Hot Corrosion of Nickel-Base Alloys. Metall. Trans., vol. 4, Jan. 1973, pp. 261-278.
8. Semchishen, M.: Molybdenum in Heat Resistant Nickel-base Alloys. Met. Sci. Heat Treat., vol. 15, no. 7-8, Jan. 1974, pp. 569-571.
9. Peters, K. R.; Whittle, D. P.; and Stringer, J.: Oxidation and Hot Corrosion of Nickel-Based Alloys Containing Molybdenum. Corros. Sci., vol. 16, no. 11, 1976, pp. 791-804.
10. Morrow, Hugh, III.; Sponseller, D. L.; and Kalns, E.: The Effects of Molybdenum and Aluminum on the Hot Corrosion (Sulfidation) Behavior of Experimental Nickel-Base Superalloys. Metall. Trans., vol. 5, no. 3, Mar. 1974, pp. 673-683.
11. Yang, S. W.: Effect of Ti and Ta on the Oxidation of a Complex Superalloy. Report No. 80CRD041, General Electric Co., 1980.
12. Reising, R. F.: Effects of Chromium, Molybdenum and Tungsten on Sodium Sulfate-Induced High Temperature Corrosion on Nickel. Corrosion, vol. 31, May 1975, pp. 159-163.
13. Deadmore, Daniel L.: Application of Induction Coil Measurements to the Study of Superalloy Hot Corrosion and Oxidation. NASA TM-83560, 1984.
14. Barrett, C. A.; Miner, R. V., and Hull, D. R.: The Effects of Cr, Al, Ti, Mo, W, Ta, and Nb on the Cyclic Oxidation Behavior of Cast Ni-Based Alloys at 1100 to 1150 C. Oxidation of Metals, vol. 20, no. 5/6, pp. 255-272, 1983.
15. Lowell, Carl E.; and Deadmore, Daniel L.: The Kinetics of High Velocity, High Temperature Corrosion of U700. Presented at 162nd Fall Meeting of Electrochemical Society (Detroit, Mich.), Oct. 17-21, 1982.
16. Misra, A. K,; and Kohl, F. J.: Effect of the Amount of Na_2SO_4 on the High Temperature Corrosion of Udimet-700. NASA TM-83459, 1983.

1. Report No.	2. Government Accession No.	3. Recipient's Catalog No.
NASA TP-2338		

4. Title and Subtitle	5. Report Date
Effects of Alloy Composition on Cyclic Flame Hot-Corrosion Attack of Cast Nickel-Base Superalloys at 900° C	July 1984
	6. Performing Organization Code: 505-33-1A
7. Author(s): Daniel L. Deadmore	8. Performing Organization Report No.: E-2009
	10. Work Unit No.
9. Performing Organization Name and Address: National Aeronautics and Space Administration, Lewis Research Center, Cleveland, Ohio 44135	11. Contract or Grant No.
	13. Type of Report and Period Covered: Technical Paper
12. Sponsoring Agency Name and Address: National Aeronautics and Space Administration, Washington, D.C. 20546	14. Sponsoring Agency Code

15. Supplementary Notes

16. Abstract

The effects of Cr, Al, Ti, Mo, Ta, Nb, and W content on the hot corrosion of nickel-base alloys were investigated. The alloys were chosen to cover nearly the range of commercial alloy compositions. They were tested in a Mach 0.3 flame with 0.5 ppmw sodium at a temperature of 900° C. The degree of attack was estimated by four methods: change in metal diameter, loss of cross-sectional area, descaled weight loss, and change in the inductance of a solenoid coil with a test sample as a core. The first three measurements are destructive and were made only at the end of testing (300 1-hr cycles). The coil measurement is a nondestructive method. By using coil measurements the corrosion resistance of these alloys could be predicted from short-time testing. The best corrosion resistance was achieved when the Cr content was >12 wt %. However, some lower-Cr-content alloys (<10 wt %) exhibited reasonable resistance provided that the Al content was <2.5 wt % and the Ti content was <4 wt %. The effects of W, Ta, Mo, and Nb contents on the hot-corrosion resistance varied depending on the Al and Ti contents. Several commercial alloy compositions were also tested and the corrosion attack was measured. Predicted attack was calculated for these alloys from derived regression equations and was in reasonable agreement with that experimentally measured. The regression equations were derived from measurements made on alloys in a one-quarter replicate of a 2^7 statistical design alloy composition experiment. These regression equations represent a simple linear model and are only a very preliminary analysis of the data needed to provide insights into the experimental method.

17. Key Words (Suggested by Author(s))	18. Distribution Statement
Nickel alloys Hot corrosion Cobalt alloys	Unclassified - unlimited STAR Category 26

19. Security Classif. (of this report)	20. Security Classif. (of this page)	21. No. of pages	22. Price*
Unclassified	Unclassified	29	A03

*For sale by the National Technical Information Service, Springfield, Virginia 22161

NASA-Langley, 1984

National Aeronautics and
Space Administration

Washington, D.C.
20546

Official Business
Penalty for Private Use, $300

THIRD-CLASS BULK RATE

Postage and Fees Paid
National Aeronautics and
Space Administration
NASA-451

NASA

POSTMASTER: If Undeliverable (Section 158 Postal Manual) Do Not Return